AD-A038 518 ILLINOIS UNIV AT URBANA-CHAMPAIGN DEPT OF ELECTRICAL --ETC F/G 20/5
FREQUENCY TUNABLE LASER SOURCES.(U)
MAR 77 P D COLEMAN AF-AFOSR-2988
UNCLASSIFIED UILU-ENG-77-2548 AFOSR-TR-77-0379 NL

1 OF 2
AD A038 518

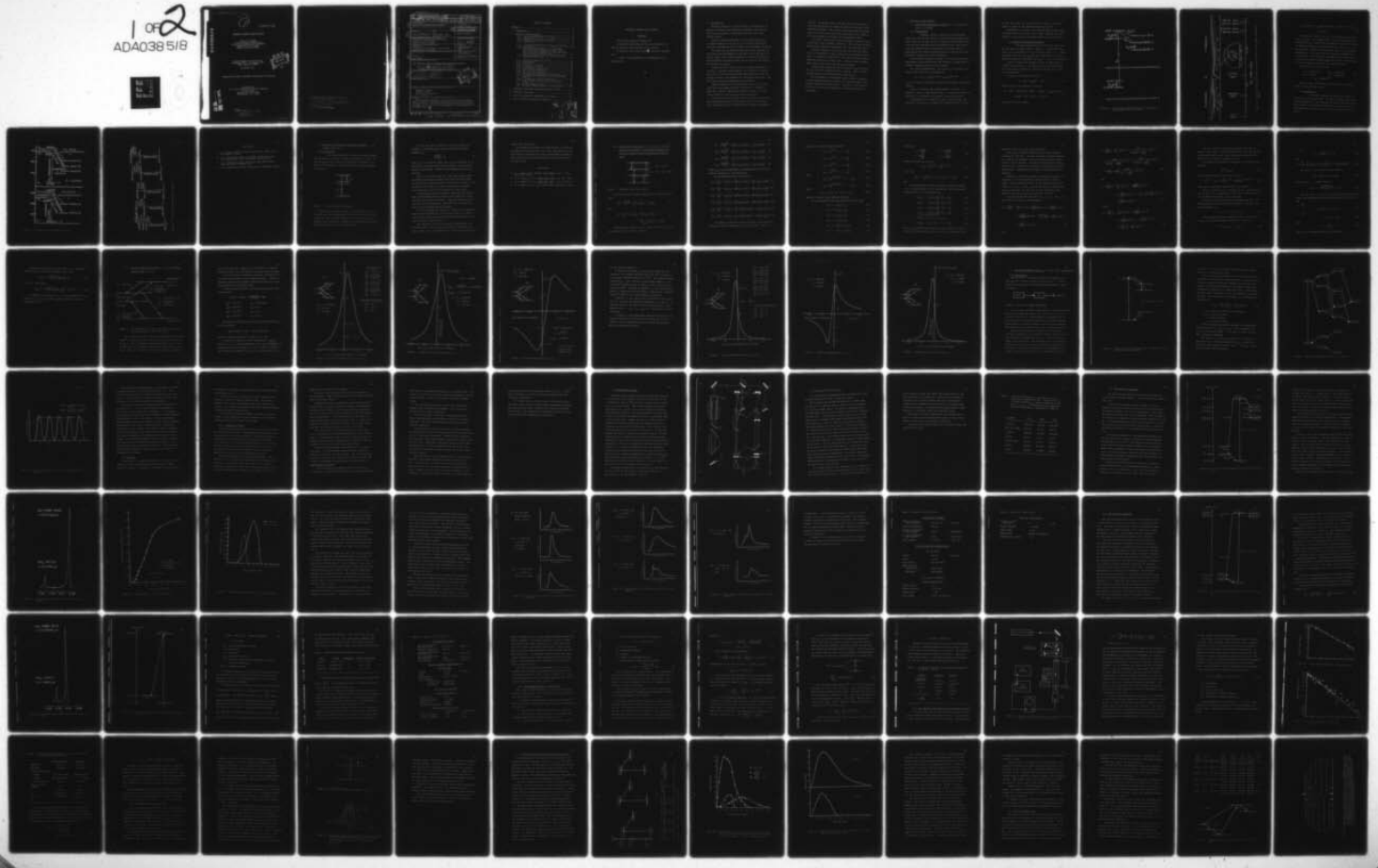

UILU-ENG-77-2548

FREQUENCY TUNABLE LASER SOURCES

Paul D. Coleman
Electro-Physics Laboratory
Electrical Engineering Department
University of Illinois
Urbana, Illinois 61801

Interim Report for the period
1 February 1976 - 31 January 1977
Grant AFOSR 76-2988

21 March 1977

Approved for public release; distribution unlimited.

Prepared for
Air Force Office of Scientific Research
Building 410
Bolling Air Force Base
Washington, D.C. 20332

AIR FORCE OFFICE OF SCIENTIFIC RESEARCH (AFSC)
NOTICE OF TRANSMITTAL TO DDC
This technical report has been reviewed and is approved for public release IAW AFR 190-12 (7b).
Distribution is unlimited.
A. D. BLOSE
Technical Information Officer

UNCLASSIFIED

SECURITY CLASSIFICATION OF THIS PAGE (When Data Entered)

(18) (19) **REPORT DOCUMENTATION PAGE** (9)

READ INSTRUCTIONS BEFORE COMPLETING FORM

1. REPORT NUMBER: AFOSR-TR-77-0379	2. GOVT ACCESSION NO. / Interim Rept. 2 Jan 76-31 Jan 77	3. RECIPIENT'S CATALOG NUMBER
4. TITLE (and Subtitle): FREQUENCY TUNABLE LASER SOURCES. (6)	5. TYPE OF REPORT & PERIOD COVERED: Interim 2-1-76/1-31-77
	6. PERFORMING ORG. REPORT NUMBER: UILU-ENG-77-2548 (14)
7. AUTHOR(s): (10) Paul D. Coleman (11) 21 Mar 77	8. CONTRACT OR GRANT NUMBER(s): AFOSR 76-2988 new
9. PERFORMING ORGANIZATION NAME AND ADDRESS: Electrical Engineering Department, University of Illinois, Urbana, Illinois 61801	10. PROGRAM ELEMENT, PROJECT, TASK AREA & WORK UNIT NUMBERS: 9751-02 61102F
11. CONTROLLING OFFICE NAME AND ADDRESS: AFOSR/NP, Building 410, Bolling Air Force Base, Washington, D.C. 20332	12. REPORT DATE: March 21, 1977
	13. NUMBER OF PAGES: 103
14. MONITORING AGENCY NAME & ADDRESS (if different from Controlling Office) (12) 106p.	15. SECURITY CLASS. (of this report): UNCLASSIFIED
	15a. DECLASSIFICATION/DOWNGRADING SCHEDULE

16. DISTRIBUTION STATEMENT (of this Report)

Approved for public release; distribution unlimited.

(15) ✓ AF-AFOSR-2988

17. DISTRIBUTION STATEMENT (of the abstract entered in Block 20, if different from Report)

(16) 9751 (17) 02

DDC Reproduced APR 19 1977 C

18. SUPPLEMENTARY NOTES

19. KEY WORDS (Continue on reverse side if necessary and identify by block number)

Molecular lasers
Tunable lasers
Four wave interaction
Far infrared

20. ABSTRACT (Continue on reverse side if necessary and identify by block number)

This report describes research on a) optically pumped NH_3 and PH_3 with particular attention given to the 12.08 and 11.46 μm lines, b) four-wave four-level nonlinear molecular systems, and c) laser line assignments in the important far IR CH_3OH laser.

DD FORM 1 JAN 73 1473 EDITION OF 1 NOV 65 IS OBSOLETE

176 009

UNCLASSIFIED

SECURITY CLASSIFICATION OF THIS PAGE (When Data Entered)

TABLE OF CONTENTS

FREQUENCY TUNABLE LASER SOURCES

Abstract

This report describes research on

a) optically pumped NH_3 and PH_3 with particular attention given to the 12.08 and 11.46 μm lines,

b) four-wave four-level nonlinear molecular systems, and,

c) laser line assignments in the important far IR CH_3OH laser.

1. INTRODUCTION

The basic objective of this contract is exploratory research on technical and engineering problems in the far IR that will be important in developing the area for future relevant needs.

Specific problems described in this annual report are 1) optical pumping of NH_3 and PH_3, 2) four-wave four-level nonlinear interactions, and 3) laser line assignments in CH_3OH.

The spherical top molecules NH_3 and PH_3 are important in that they uield wavelengths of interest, yield high power, efficient laser lines, lasing transitions are both V-R and R-R, and interesting nonlinear effects can be realized with single and multiple CO_2 pumps.

Studies on the 12.08 and 11.46 μm of NH_3, optically excited in a capillary tube geometry, are described in detail. The 11.46 μm line strongly suggests Raman behavior since the emission occurs in the absence of a population inversion. The 12.08 has interesting superfluorescent behavior.

Optical pumping of far IR molecular lasers for the past seven years has essentially been confined to a single CO_2 pump and a two-wave three-level system. Moreover, only the linear behavior of the system has been considered.

In the latter half of this contract period, an analytical and experimental study of a four-wave four-level system has been initiated which will include linear, Raman and parametric

effects. The density matrix has been used for the analysis with both analytical and numerical computer solutions of the equations obtained. Four levels in NH_3 have been identified that will closely match three CO_2 laser pump lines. Hence a well-known system is available for experimental study.

Four-level systems will permit frequency conversion, both up and down, plus frequency tunability. The nonlinear effects might also be used as a diagnostic tool for molecular gases.

Methanol (CH_3OH) is at the present time the most important far IR molecule in that, along with its deuterated varities, it accounts for some 25% of all known optically pumped molecular laser far IR laser lines. However, until December 1976, none of the laser lines has been assigned.

A CH_3OH laser system had been developed on this contract for use in far IR integrated optics studies. Hence a direct interest existed to understand this CH_3OH system.

The assignment of 13 important CH_3OH lines is presented in this report along with reference to a detailed paper that has been accepted for publication. Molecules, with internal rotation, are excellent candidates for optically pumped far IR systems.

2. TECHNICAL ACCOMPLISHMENTS

2.1 Laser Line Assignments in CH_3OH - E. J. Danielewicz and P. D. Coleman

2.11 Introduction

Methanol (CH_3OH), along with its deuterated varieties, accounts for 25% of all known optically pumped molecular laser far IR laser lines.[1] However, none of these laser lines had been assigned, prior to December 1976, when Danielewicz and Coleman[2] from the University of Illinois and J. O. Henningsen[3] from Denmark presented papers at the San Juan Submillimeter Conference on the assignments.

The assignment problem in CH_3OH is the lack of sufficient spectroscopic data and the fact the spectrum is complicated by hindred internal rotation of the OH group.

To a first approximation, the energy E_v of a ground electronic state level can be expressed as

$$E_v = G(v) + E_v(JK)^{\text{ext rot}} + E_v(n\tau K)^{\text{int rot}} \qquad (1)$$

i.e., as a sum of vibrational, external and internal rotational energy.

Hence it requires five quantum numbers (v,J,K,n,τ) to identify a level in the simplest case. If asymmetry and A-state splitting is considered, the problem is more complicated.

Fortunately D. R. Woods[4] did a Ph.D. thesis on the high resolution IR spectra of methanol in the 400-1300 cm^{-1} region

in 1970 from which one can get sufficient data to at least assign a number of the important CH_3OH laser lines.

Assignment on 13 laser lines has been made, a paper given in December 1976 at San Juan, and a paper accepted for publication in IEEE Journal of Quantum Electronics for June 1977.

2.12 Summary of Assignment Technique

The pump absorption and far IR laser lines follow the general pattern shown in Figure 1. A particular CO_2 laser line is absorbed on an R_a transition from 0 - ν_5. Lasing typically occurs on R_{oa}, R_{ob} and Q_{ob} transitions in ν_5, with possible additional cascading like R_{sa} or $\nu = 0$ $R_{\tau a}$ transitions.

Figure 2 displays an absorption curve of CH_3OH taken at -50°C to display only n = 0 transitions along with selected CO_2 lines that are absorbed. Comparing the data will permit J to be evaluated.

An $R_a(J-1)$ transition is given by

$$\nu_a = 2BJ - 2D_{JK}JK^2 - 4D_JJ^3 \tag{2}$$

while an $R_b(J-1)$ transition is given by

$$\nu_b = 2BJ + (2K-1)(A-B) - 4D_JJ^3 - 2D_{JK}JK^2 - D_{JK}J(J-1)(2K-1) - D_K[4K^3 - 6K^2 + 3K-1] + \Delta F_{\nu_2}(n_\tau K) \tag{3}$$

and a $Q_b(J)$ by the formula

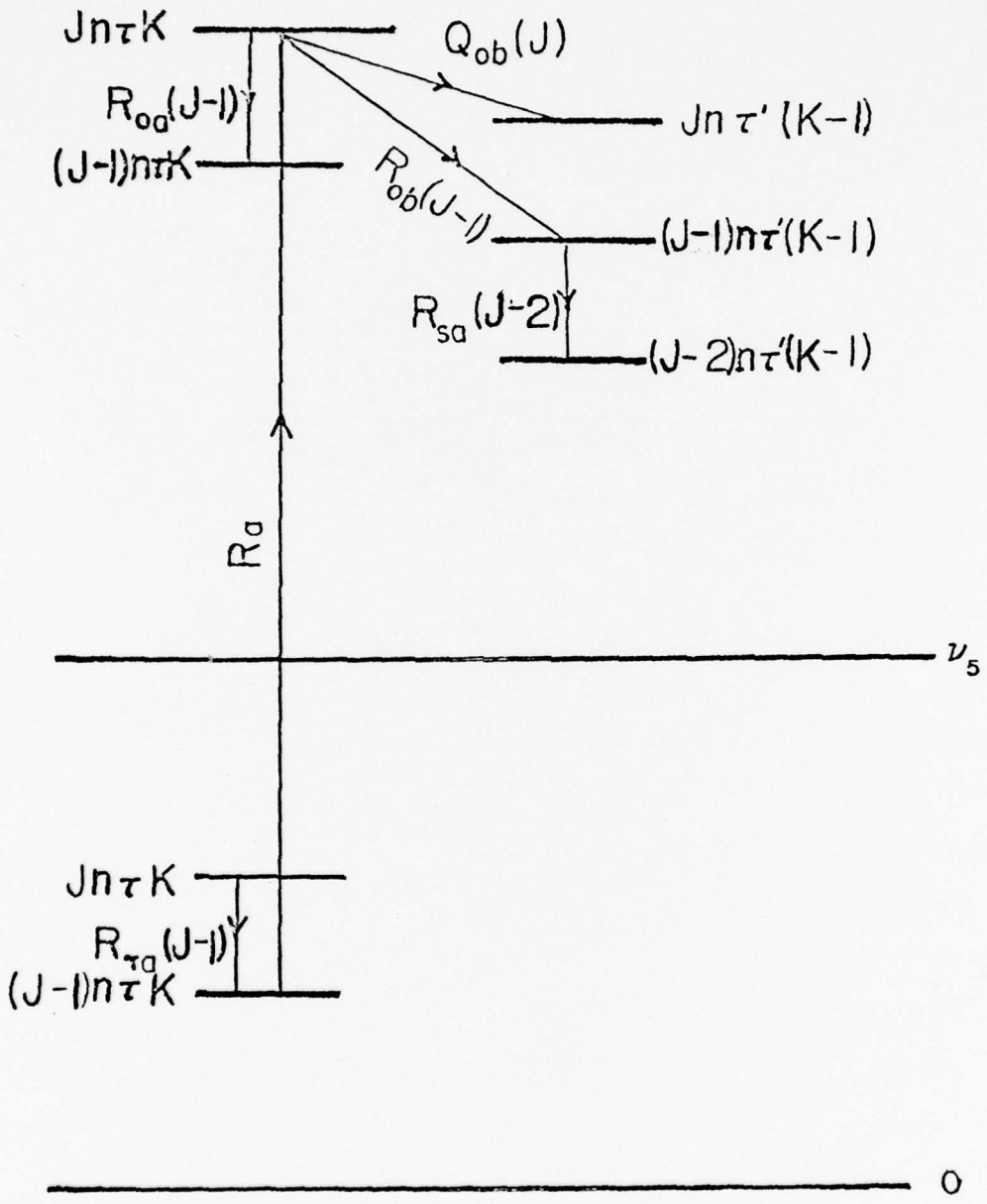

Figure 1. A few of the possible FIR lasing transitions in CH_3OH pumped with a CO_2 laser.

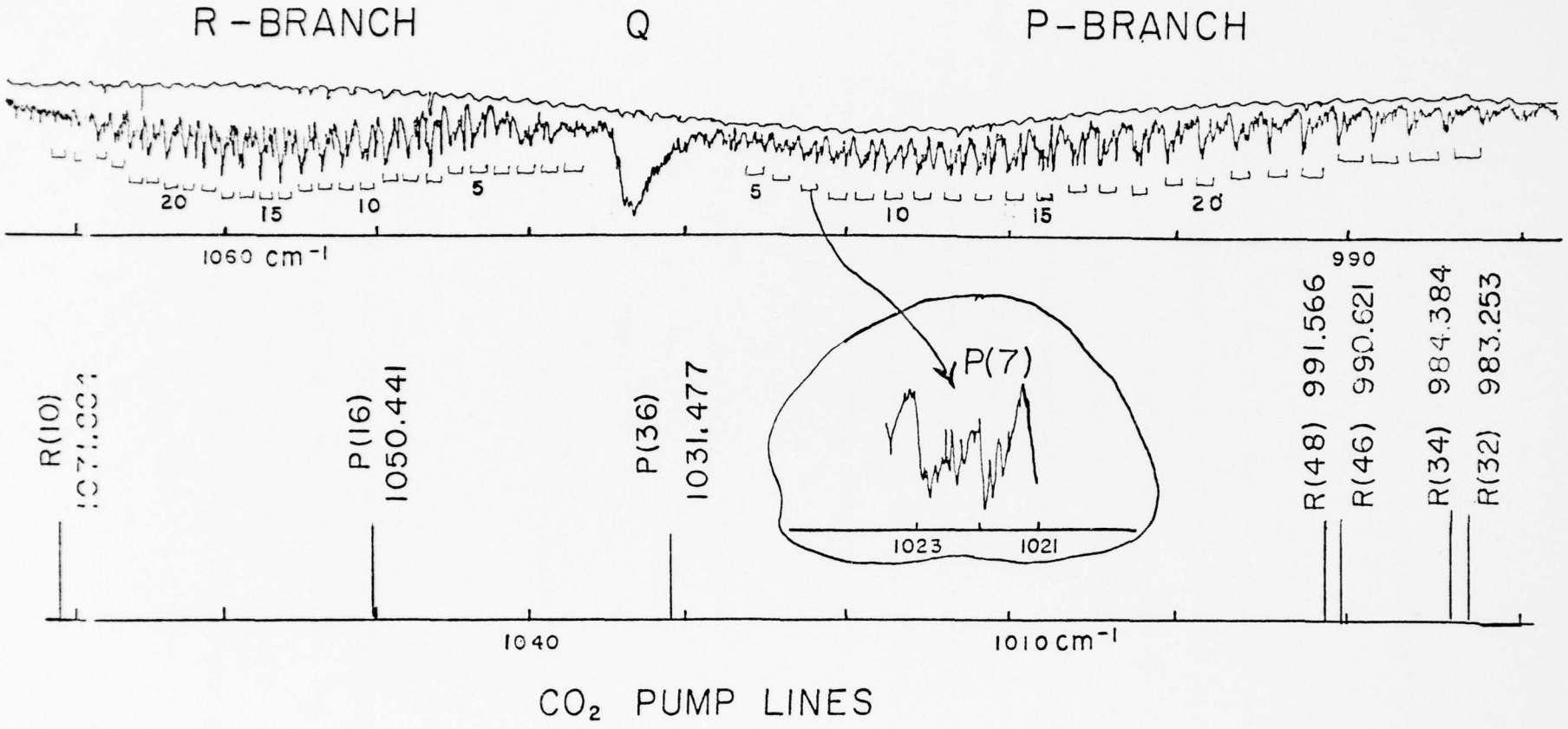

Figure 2. CH_3OH-CO stretch, absorption spectrum (@-50°C) with CO_2 pump lines superimposed.

$$\nu_b = (2K-1)(A-B) - D_{JK}J(J+1)(2K-1) - D_K[4K^3 - 6K^2 + 4K-1] + \Delta F_{\nu_2}(n_\tau K) \quad (4)$$

Woods gives a table of $E_{\nu_2}(n\ K)$ from which one can determine $\Delta E_{\nu_2}(n_\tau K)$. The constants were initially known with sufficient accuracy to make first assignments, using the criterion of frequency matching, polarization of the signal ($\parallel$ or $\perp$ to the CO_2 pump), cascade and competition effects and frequency consistencies. One could also use transition probabilities to advantage. After the first assignments, one could then in turn use the accurate laser frequencies to make a least square fit of the constants to obtain more accurate values.

The result of this effort was

$$\begin{aligned} B &= 0.7999\ cm^{-1} & D_{JK} &= 3.8830\times10^{-5} \\ A-B &= 3.4124 & D_J &= 7.3823\times10^{-7} \\ & & D_K &= 3.008\times10^{-4} \end{aligned} \quad (5)$$

Figures 3 and 4 pictorially give the laser line assignments of 13 CH_3OH laser lines.

2.13 Conclusions

The present assignments should have impact on the theory of the CH_3OH laser. It should stimulate additional Stark measurements on the molecule and double resonance studies. CH_3OH serves as the simplest example of the desirability of molecules with internal rotation as laser candidates for the far IR.

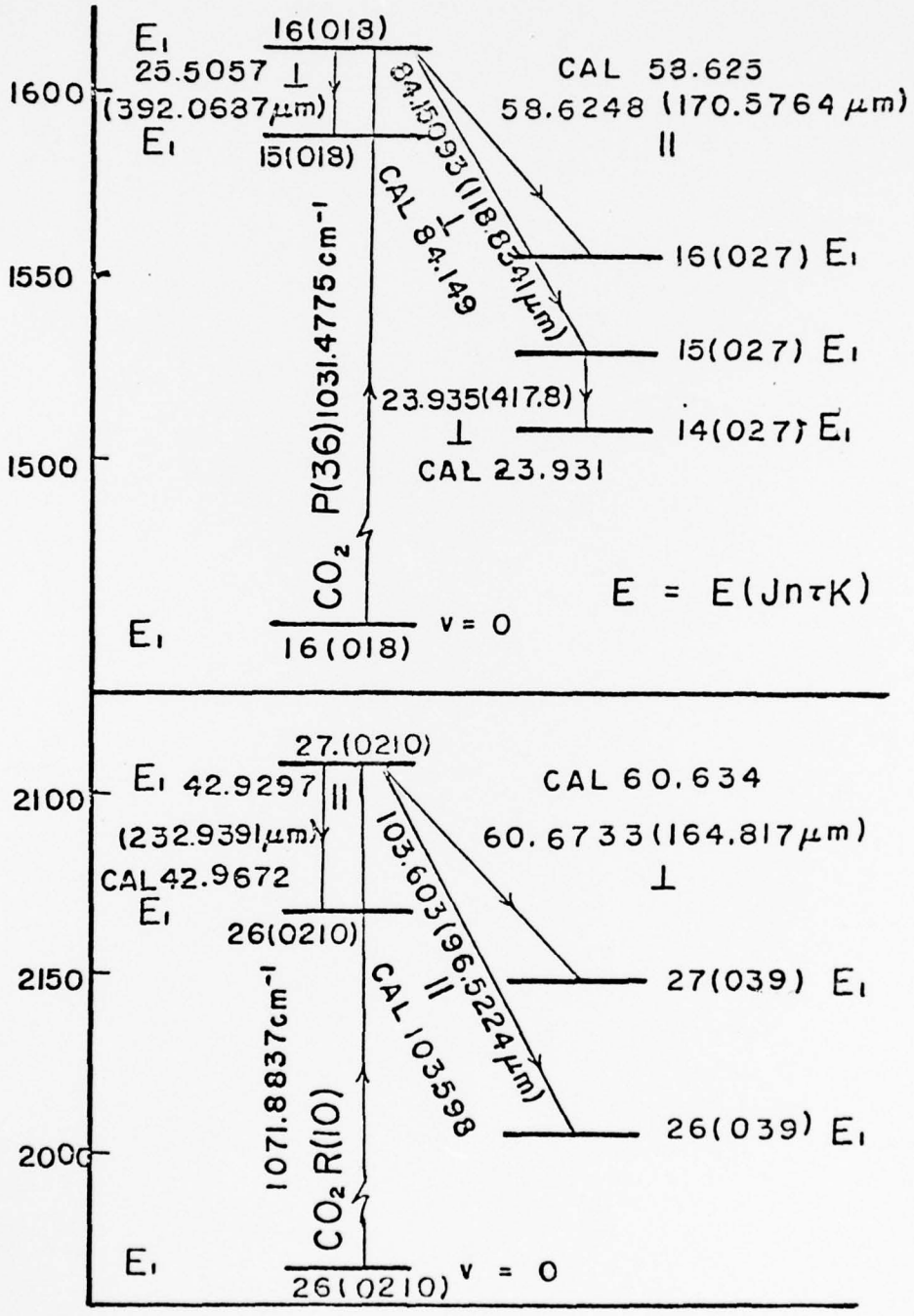

Figure 3. FIR laser line assignments in CH_3OH.

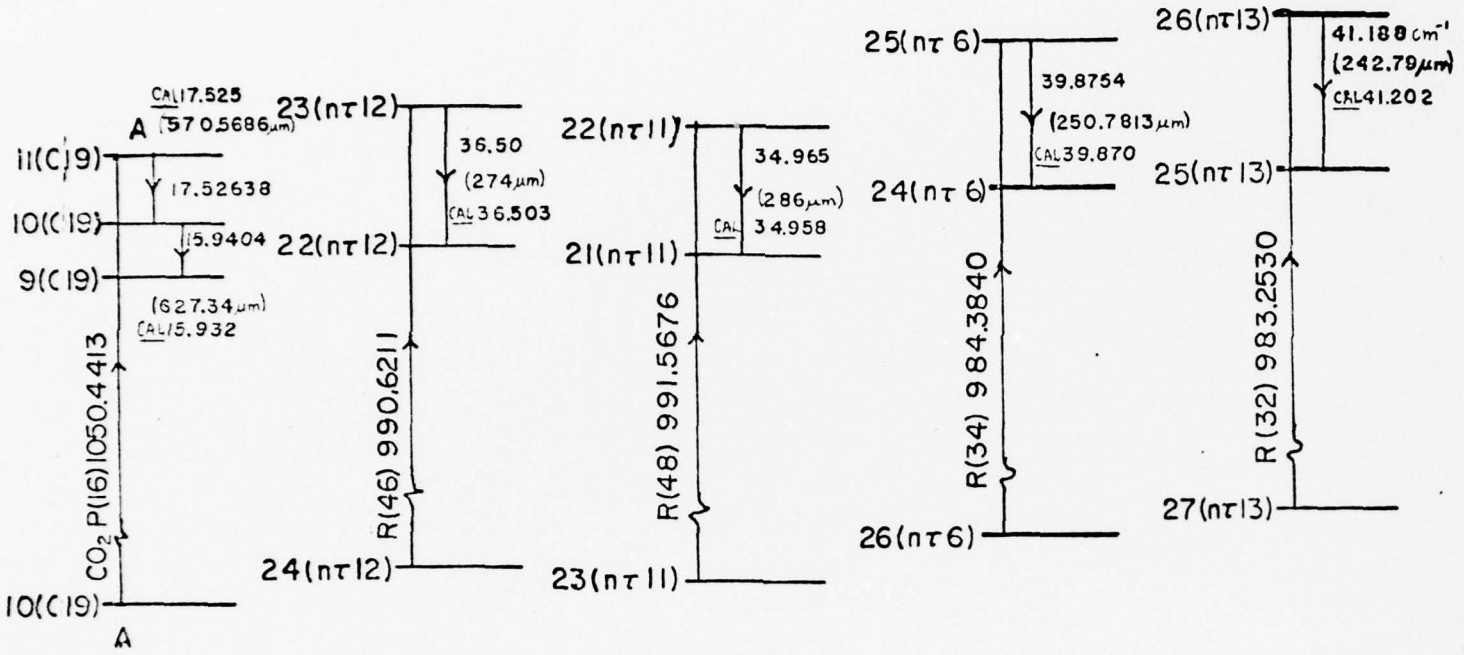

Figure 4. FIR laser line assignments in CH_3OH.

References

1. M. Yamanaka, "Review of Laser Engineering, Japan, Vol. 3, pp. 253-294, (1976).

2. E. J. Danielewicz and P. D. Coleman, Paper M-3-7, San Juan Submillimeter Wave Conference, December 1976.

3. J. O. Henningsen, Paper M-3-8, San Juan Submillimeter Wave Conference, December 1976.

4. D. R. Woods, Ph.D. Thesis, University of Michigan, (1970).

2.2 Nonlinear Interactions in Molecular Systems - P. D. Coleman and W. Lee

2.21 Introduction

Optically pumped far IR molecular laser research was initiated by the work of Chang and Bridges[1] in 1970. In all the papers since then the authors have reported the behavior of essentially a two-wave three-level system as shown in Figure 1.

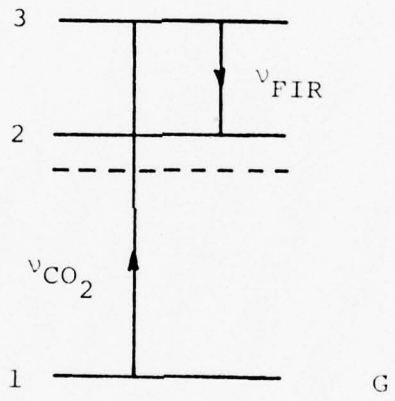

Figure 1. Two-wave three-level system.

The molecule has been pumped, via a CO_2 laser line, from a ground state to a vibrational state where the far IR lasing occurs on a pure rotational transition. Cascade rotational transition may also occur. However, few vibrational-rotational transitions have been seen and identified.

If a CO_2 TEA laser is used as a pump, the pump field strength E_p can become quite large so that the nonlinear parameter w_p

$$\left(\frac{\mu_{13}E_p}{\hbar\Delta\nu_{31}}\right) = w_p \tag{1}$$

where μ_{13} is the matrix element and $\Delta\nu_{31}$ the linewidth of the transition, can become much greater than one, and nonlinear effects should appear. However, these effects have not been reported.

The use of a single pump for a molecular system limits the number of molecular energy levels that can be accessed and the effects (linear-nonlinear) that can be realized. Also, a tunable laser source will not be achieved via cascading R-R transitions, since the R-R spacing are about equal.

Considerations of this kind have suggested that multiple laser pump systems should be studied with respect to linear, nonlinear and parametric effects. Four-wave four-level systems have been experimentally studied[2-4] but a detailed analysis of these systems has not appeared.

In the following two sections an analytical and numerical density matrix analysis of a four-level system is presented. This system includes two-wave three-level and three-wave four-level systems as special cases.

The analytical work is not entirely completed but the difficult part of the problem (derivation of formulas, computer coding, etc.) is complete and to the point of displaying

initial data and results.

An experimental problem, not reported here, critical to synchronizing the pulses from 2 or 3 CO_2 TEA lasers has also been solved by replacing the usual gas discharge switches in these lasers by high voltage hydrogen thyratrons which have far less jitter.

References

1. T. Y. Chang and T. Bridges, Opt. Commun., Vol. 1, 423-425, April (1970).

2. P. P. Sorokin, et al., Appl. Phys. Lett., 22, 342 (1972).

3. R. T. Hodgson, et al., Phys. Rev. Lett., 32, 373 (1973).

4. J. J. Wynne, et al., Proc. Laser Spect. Conference, (1973).

2.22 Density Matrix Analysis of a Four-Wave Four-Level System Which Includes a Three-Wave Four-Level System and a Two-Wave Three-Level System as Special Cases

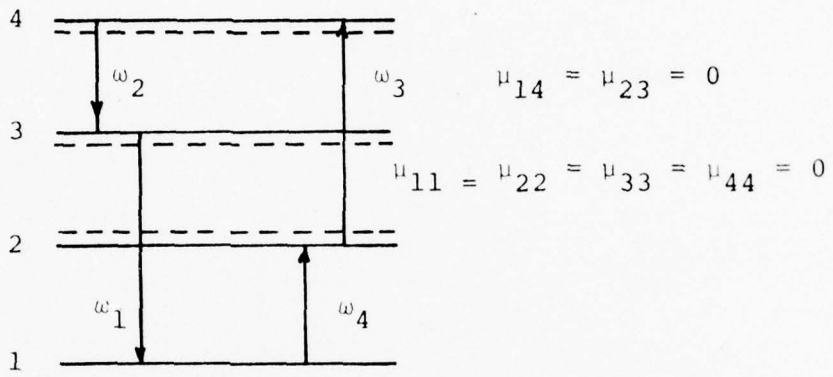

Figure 1. Four-wave four-level system.

The general density matrix equations will be taken in the form

$$\dot{\rho}_{nn} + \frac{\rho_{nn} - \rho_{nn}^{e}}{T_1} = \frac{1}{ih} \sum_{k} \left(H'_{nk}\rho_{kn} - \rho_{nk}H'_{kn} \right) \tag{1}$$

and

$$\dot{\rho}_{nm} + \left(\frac{1}{T_2} - i\Omega_{mn} \right) \rho_{nm} = \frac{1}{ih}(\rho_{mm} - \rho_{nn}) H'_{nm} + \frac{1}{ih} \sum_{k \neq n,m} \left(H'_{nk}\rho_{km} - \rho_{nk}H'_{km} \right) \tag{2}$$

Applying these equations to the system of Figure 1, yields the diagonal density matrix equations

$$\dot{\rho}_{11} + \frac{\rho_{11}-\rho_{11}^{e}}{T_1} = \frac{1}{i\hbar}\left\{(\rho_{21}-\rho_{12})H'_{12} + (\rho_{31}-\rho_{13})H'_{14}\right\} \quad (3)$$

$$\dot{\rho}_{22} + \frac{\rho_{22}-\rho_{22}^{e}}{T_1} = \frac{1}{i\hbar}\left\{(\rho_{12}-\rho_{21}(H'_{12} + (\rho_{42}-\rho_{24})H'_{24}\right\} \quad (4)$$

$$\dot{\rho}_{33} + \frac{\rho_{33}-\rho_{33}^{e}}{T_1} = \frac{1}{i\hbar}\left\{(\rho_{13}-\rho_{31})H'_{13} + (\rho_{43}-\rho_{34})H'_{34}\right\} \quad (5)$$

$$\dot{\rho}_{44} + \frac{\rho_{44}-\rho_{44}^{e}}{T_1} = \frac{1}{i\hbar}\left\{(\rho_{24}-\rho_{42})H'_{24} + (\rho_{34}-\rho_{43})H'_{34}\right\} \quad (6)$$

where ρ_{nn}^{e} is the thermodynamic equilibrium value and the dot notation represents a time derivation.

The off-diagonal matrix equations are

$$\dot{\rho}_{12} + \left(\frac{1}{T_2} - i\Omega_{21}\right)\rho_{12} = \frac{1}{i\hbar}(\rho_{22}-\rho_{11})H'_{12} + \frac{1}{i\hbar}[\rho_{32}H'_{13}-\rho_{14}H'_{24}] \quad (7)$$

$$\dot{\rho}_{13} + \left(\frac{1}{T_2} - i\Omega_{31}\right)\rho_{13} = \frac{1}{i\hbar}(\rho_{33}-\rho_{11})H'_{13} + \frac{1}{i\hbar}[\rho_{23}H'_{12}-\rho_{14}H'_{43}] \quad (8)$$

$$\dot{\rho}_{24} + \left(\frac{1}{T_2} - i\Omega_{42}\right)\rho_{24} = \frac{1}{i\hbar}(\rho_{44}-\rho_{22})H'_{24} + \frac{1}{i\hbar}[\rho_{14}H'_{21}-\rho_{23}H'_{34}] \quad (9)$$

$$\dot{\rho}_{34} + \left(\frac{1}{T_2} - i\Omega_{43}\right)\rho_{34} = \frac{1}{i\hbar}(\rho_{44}-\rho_{33})H'_{34} + \frac{1}{i\hbar}[\rho_{14}H'_{31}-\rho_{32}H'_{24}] \quad (10)$$

$$\dot{\rho}_{14} + \left(\frac{1}{T_2} - i\Omega_{41}\right)\rho_{14} = \frac{1}{i\hbar}\,[\rho_{24}H'_{12}-\rho_{12}H'_{24} + \rho_{34}H'_{13}-\rho_{13}H'_{34}] \quad (11)$$

$$\dot{\rho}_{23} + \left(\frac{1}{T_2} - i\Omega_{32}\right)\rho_{23} = \frac{1}{i\hbar}\,[\rho_{13}H'_{21}-\rho_{21}H'_{13} + \rho_{43}H'_{34}-\rho_{24}H'_{43}] \quad (12)$$

In seeking a solution to these equations, only terms containing a resonant denominator will be retained. This will

permit the following assumed solutions

$$\rho_{13} = \lambda_1 e^{i\omega_1 t} + ... = \rho_{31}^* \tag{13}$$

$$\rho_{34} = \lambda_2 e^{i\omega_2 t} + ... = \rho_{43}^* \tag{14}$$

$$\rho_{24} = \lambda_3 e^{i\omega_3 t} + ... = \rho_{42}^* \tag{15}$$

$$\rho_{12} = \lambda_4 e^{i\omega_4 t} + ... = \rho_{21}^* \tag{16}$$

with

$$\rho_{14} = D_1 e^{i(\omega_3+\omega_4)t} + ... = \rho_{41}^* \tag{17}$$

$$\rho_{23} = D_2 e^{i(\omega_3-\omega_2)t} + ... = \rho_{32}^* \tag{18}$$

where

$$\omega_1+\omega_2 = \omega_3+\omega_4 \quad \text{or} \quad \omega_3-\omega_2 = \omega_1-\omega_4 \tag{19}$$

and the * notation means complex conjugate.

It is convenient to use the following defined terms

$$R_1 = 1 + iT_2(\omega_1-\Omega_{31}) \tag{20}$$

$$R_2 = 1 + iT_2(\omega_2-\Omega_{43}) \tag{21}$$

$$R_3 = 1 + iT_2(\omega_3-\Omega_{42}) \tag{22}$$

$$R_4 = 1 + iT_2(\omega_4-\Omega_{21}) \tag{23}$$

$$R_5 = 1 + iT_2(\omega_3+\omega_4-\Omega_{41}) \tag{24}$$

$$R_6 = 1 + iT_2(\omega_3-\omega_2-\Omega_{32}) \tag{25}$$

along with

$$a = \frac{\mu_{12}E_4T_2}{2\hbar} \qquad b = \frac{\mu_{24}E_3T_2}{2\hbar}$$
$$c = \frac{\mu_{43}E_2T_2}{2\hbar} \qquad d = \frac{\mu_{12}E_1T_2}{2\hbar} \tag{26}$$

where the fields are taken as

$$E(\omega_1) = \frac{E_1}{2} e^{i\omega_1 t} + \frac{E_1^*}{2} e^{-i\omega_1 t} \tag{27}$$

etc., and

$$H'_{12} = -\mu_{12}\left[E(\omega_1) + E(\omega_2) + E(\omega_3) + E(\omega_4)\right] \tag{28}$$

etc.

Using these abbreviations and making a harmonic balance (i.e., equating terms of like frequencies), the off-diagonal equations are of the following form.

$$iR_1\lambda_1 = -d(\rho_{33}^\circ - \rho_{11}^\circ) + C^*D_1 - aD_2 \tag{29}$$

$$iR_2\lambda_2 = -c(\rho_{44}^\circ - \rho_{33}^\circ) - d^*D_1 + bD_2^* \tag{30}$$

$$iR_3\lambda_3 = -b(\rho_{44}^\circ - \rho_{22}^\circ) - a^*D_1 + cD_2 \tag{31}$$

$$iR_4\lambda_4 = -a(\rho_{22}^\circ - \rho_{11}^\circ) + b^*D_1 - dD_2^* \tag{32}$$

$$iR_5D_1 = c\lambda_1 - d\lambda_2 - a\lambda_3 + b\lambda_4 \tag{33}$$

$$iR_6D_2 = -a^*\lambda_1 - b\lambda_2^* + c^*\lambda_3 + d\lambda_4^* \tag{34}$$

where ρ_{nn}° represents the steady state (DC) population and the dotted lines indicate the linear form of the equations if the

nonlinear terms in D_1 and D_2 were neglected.

There are six complex unknowns (twelve real unknowns) in Equations (29)-(34). Six more equations could be obtained by * each of the equations to yield essentially twelve equations in twelve unknowns. Although the determinants contain many zeros, it would be very tedious to solve these equations analytically. Numerically they could be solved readily on a computer.

However, it would be desirable to display an analytical solution, if a good approximate solution could be readily found. This can easily be done, if one uses the linear solutions for λ_1, λ_2, λ_3, and λ_4 in the nonlinear D_1 and D_2 terms given by Equations (33) and (34) and then substitute these values for D_1 and D_2 back into Equations (29)-(32).

The good approximate solutions for λ_1, λ_2, λ_3, and λ_4 are then seen to be given by the expressions

$$\left(1 + \frac{a^2}{R_1 R_6}\right)\lambda_1 \simeq \frac{id}{R_1}(\rho_{33}^{\circ}-\rho_{11}^{\circ}) + \frac{ic^2 d}{R_1 R_2 R_5}(\rho_{44}^{\circ}-\rho_{33}^{\circ}) - \frac{ia^2 d}{R_1 R_4^{*} R_6}(\rho_{22}^{\circ}-\rho_{11}^{\circ})$$

$$+ i\,\frac{abc^{*}}{R_1 R_2^{*} R_6}(\rho_{44}^{\circ}-\rho_{33}^{\circ}) + i\,\frac{abc^{*}}{R_3}\left(\frac{1}{R_1 R_5} + \frac{1}{R_1 R_6}\right)(\rho_{44}^{\circ}-\rho_{22}^{\circ})$$

$$- i\,\frac{abc^{*}}{R_1 R_4 R_5}\,(\rho_{22}^{\circ}-\rho_{11}^{\circ}) \qquad (35)$$

with

$$\left(1 + \frac{b^2}{R_2 R_6^*}\right)\lambda_2 \simeq \frac{ic}{R_2}(\rho_{44}^\circ - \rho_{33}^\circ) - \frac{ib^2 c}{R_2 R_3 R_b\left(1 + \frac{a^2}{R_2 R_5}\right)}(\rho_{44}^\circ - \rho_{22}^\circ)$$

$$+ \frac{iabd^*}{R_1^* R_2 R_b^*\left(1 + \frac{a^2}{R_1^* R_6^*}\right)}(\rho_{33}^\circ - \rho_{11}^\circ) + \frac{iabd^*}{R_2 R_3 R_5\left(1 + \frac{a^2}{R_2 R_5}\right)}(\rho_{44}^\circ - \rho_{33}^\circ)$$

$$+ i\left(\frac{1}{R_2 R_5} - \frac{1}{R_2 R_6^*}\right)\frac{abd^*}{R_4\left(1 + \frac{b^2}{R_4 R_5}\right)}(\rho_{22}^\circ - \rho_{11}^\circ) \qquad (36)$$

and

$$\left(1 + \frac{a^2}{R_3 R_5}\right)\lambda_3 \simeq \frac{ib}{R_3}(\rho_{44}^\circ - \rho_{22}^\circ) - i\frac{bc^2}{R_2^* R_3 R_b}(\rho_{44}^\circ - \rho_{33}^\circ)$$

$$+ i\frac{a^2 b}{R_3 R_4 R_5}(\rho_{22}^\circ - \rho_{11}^\circ) + i\left(\frac{1}{R_5} + \frac{1}{R_6}\right)\frac{a^* cd}{R_1 R_3}(\rho_{33}^\circ - \rho_{11}^\circ)$$

$$- i\frac{a^* cd}{R_2 R_3 R_5}(\rho_{44}^\circ - \rho_{33}^\circ) \qquad (37)$$

finally

$$\left(1 + \frac{b^2}{R_4 R_5}\right)\lambda_4 \simeq \frac{ia}{R_4}(\rho_{22}^\circ - \rho_{11}^\circ) - i\frac{ad^2}{R_1^* R_4 R_6}(\rho_{33}^\circ - \rho_{11}^\circ)$$

$$+ i\frac{b^2 a}{R_3 R_4 R_5}(\rho_{44}^\circ - \rho_{22}^\circ) - i\frac{b^* cd}{R_1 R_4 R_5}(\rho_{33}^\circ - \rho_{11}^\circ)$$

$$+ i\frac{b^* cd}{R_2 R_4}\left(\frac{1}{R_5} - \frac{1}{R_6^*}\right)(\rho_{44}^\circ - \rho_{33}^\circ) \qquad (38)$$

The first terms on the RHS of Equations (35)-(38) represent linear terms. Terms containing a^2d, b^2c, c^2d, b^2a, c^2b, a^2b represent Raman terms, while the terms containing abc^*, abd^*, a^*cd, and b^*cd are parametric terms.

The complex polarization at frequency ω_2 is given by the relation

$$\frac{P_2}{2} = N\mu_{43}\lambda_2 \tag{39}$$

which from Equation (36) will have the form

$$P_2 e^{\gamma_2 z} = \varepsilon_o(\chi_e + mE_3^2)E_2 e^{\gamma_2 z} + sE_1^* E_3 E_4 e^{(\gamma_3+\gamma_4-\gamma_1^*)z} \tag{40}$$

where the z propagation factors have been inserted.

While χ_e containes E_3^2, g contains E_4^2 and s contains both E_3^2 and E_4^2 in their denominators, they are not functions of z if it is assumed these pumps are not depleted.

Notice the linear (also laser) and Raman terms have the same propagation constants but the parametric term has a possible mismatch, i.e.,

$$\Delta\gamma = \gamma_3 + \gamma_4 - \gamma_1^* - \gamma_2 \neq 0 \tag{41}$$

The polarization given by Equation (40) is the driving term in the separated Maxwell equation at frequency ω_2

$$\nabla^2 E + \omega_2^2 \mu_o \varepsilon_o E = - \omega_2^2 \mu_o P \tag{42}$$

Let

$$E = \frac{E_2(z)}{2} e^{\gamma_2 z} + cc \tag{43}$$

then

$$2\gamma_2 \frac{dE_2}{dz} + \left\{ \gamma_2^2 + \omega_2^2 \mu_o \varepsilon_o (1 + \chi_e + mE_3^2) \right\} E_2 = -\omega_2^2 \mu_o s E_1^* E_3 E_4 e^{z\Delta\gamma} \tag{44}$$

The value of γ_2^2 is found from the equation

$$\gamma_2^2 = -\omega_2^2 \mu_o \varepsilon_o [1 + (\chi_e + \gamma E_3^2)] \tag{45}$$

while for the $\Delta\delta = 0$ match condition

$$E_2(z) = -\left(\frac{\omega_2^2 \mu_o s E_1^* E_3 E_4}{2\gamma_2} \right) z + E_2(o) \tag{46}$$

Thus the terms χ_e, m and s, along with the pump fields determine the exponential and/or amplitude behavior of the system.

Let

$$\chi_e + mE_3^2 = \chi_e' - i\chi_e'' \tag{47}$$

and

$$\gamma_2 = -(\alpha_2 + ik_2) \tag{48}$$

then

$$2\alpha_2 \simeq \frac{\omega_2}{v_2} \chi_e'' \tag{49}$$

where v_2 is the phase velocity in the medium.

Exponential gain will be obtained when χ_e'' is negative. Assuming $E_2(o)$ to be zero in Equation (46), then

$$|E_2(z)|^2 = \left(\frac{\omega_2^2 \mu_o}{2}\right)^2 E_1^2 E_3^2 E_4^2 \left|\frac{s}{\gamma_2}\right|^2 z^2 \tag{50}$$

If $\Delta\gamma \neq 0$, one obtains

$$|E_2(z)|^2 = \left(\frac{\omega_2^2 \mu_o}{2}\right)^2 E_1^2 E_3^2 E_4^2 \left|\frac{s}{\gamma_2 \Delta\delta}\right|^2 |1-e^{z\Delta\gamma}|^2 \tag{51}$$

To complete the calculation of λ_2 from Equation (36), the values for ρ_{11}°, ρ_{22}°, ρ_{33}°, and ρ_{44}° must be found by solving Equations (3)-(6).

2.23 Numerical Analysis of Four-Wave Four-Level System Applied to NH_3 - W. Lee

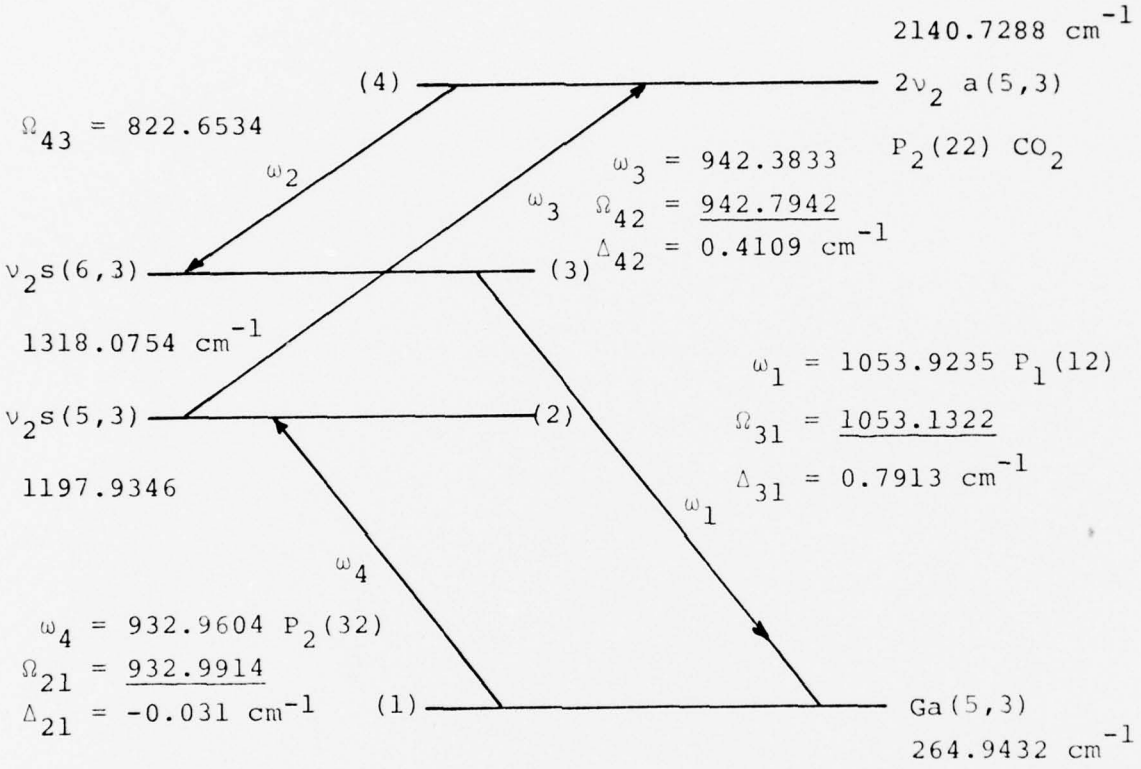

Figure 2. Four-wave four-level NH_3 system pumped with three CO_2 signals $P_1(12)$, $P_2(22)$ and $P_2(32)$.

One possible four-wave four-level system that can be pumped with two or three CO_2 laser signals is the NH_3 system shown in Figure 2. The Ω_{21} frequency match with the CO_2 line is good but the Ω_{42} and Ω_{31} frequency matches are rather far off resonance. This will mean that a substantial resonant enhancement

will not be realized. However, it is difficult to find any system for study with only discrete CO_2 laser lines available.

It was seen that an analytical solution of Equations (3)-(12) were very tedious for the steady state case. However a numerical steady state, harmonic balance solution using a CDC Syber computer is relatively simple.

In this computer solution, the following numerical data has been used.

$$T_1(\text{sec}) = T_2(\text{sec}) = \frac{1.075\times10^{-8}}{P(\text{torr})} \text{ HWHM} \tag{1}$$

$$\rho_{11}^e = 2.93\times10^{-2} \qquad \mu_{12} = 0.13 \text{ debye}$$

$$\rho_{22}^e = 2.95\times10^{-2} \qquad \mu_{24} = 0.15$$

$$\rho_{33}^e = 1.65\times10^{-4} \qquad \mu_{43} = 0.16$$

$$\rho_{44}^e = 2.86\times10^{-6} \qquad \mu_{13} = 0.14$$

The value of E_i^2 has been related to the power density P_i by the expression

$$E_i^2(\text{volts/cm})^2 = 2\eta P_i \simeq 754\ P_i(\text{watts/cm}^2) \tag{2}$$

where the medium impedance η is taken as 377 ohms.

Figures 1, 2, and 3 are three representative computer curves of χ_e', χ_e'' and the parametric term $(\omega_2^2\mu_o/2)^2E_1^2E_3^2E_4^2|s/\gamma_2|^2$ associated with the frequency $\omega_2 = 2\pi\nu_2$, versus the number of half widths off resonance $T_2(\nu_2-\gamma_{43})$, for fixed values of P_3,

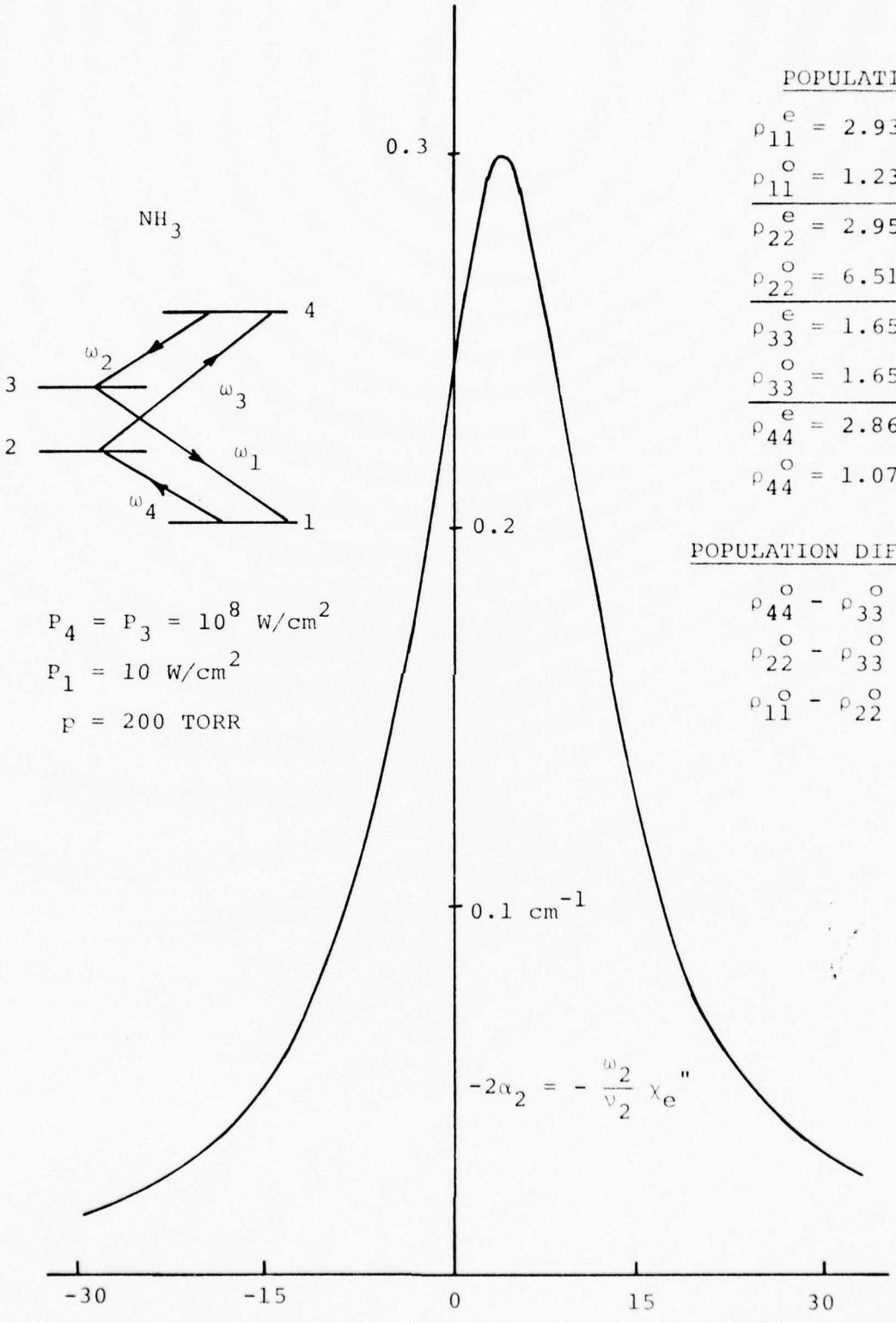

POPULATIONS [26]

$\rho_{11}^{e} = 2.93\times10^{-2}$

$\rho_{11}^{o} = 1.238\times10^{-2}$

$\rho_{22}^{e} = 2.95\times10^{-2}$

$\rho_{22}^{o} = 6.512\times10^{-3}$

$\rho_{33}^{e} = 1.65\times10^{-4}$

$\rho_{33}^{o} = 1.65\times10^{-4}$

$\rho_{44}^{e} = 2.86\times10^{-6}$

$\rho_{44}^{o} = 1.070\times10^{-2}$

POPULATION DIFFERENCES

$\rho_{44}^{o} - \rho_{33}^{o} > 0$

$\rho_{22}^{o} - \rho_{33}^{o} > 0$

$\rho_{11}^{o} - \rho_{22}^{o} > 0$

Figure 1. Linear plus Raman gain term $-2\alpha_2$ at ω_2.

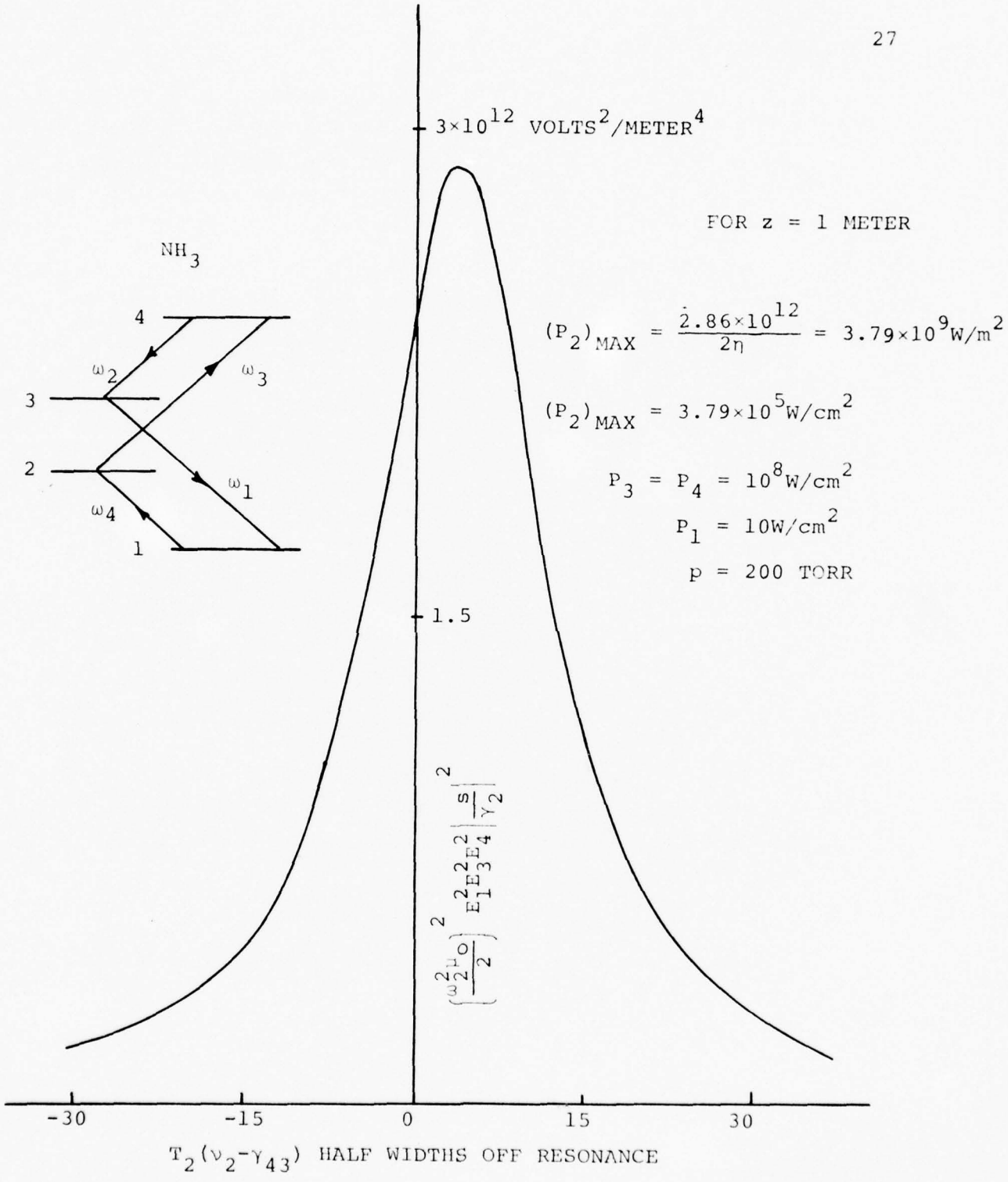

Figure 2. Parametric term associated with ω_2.

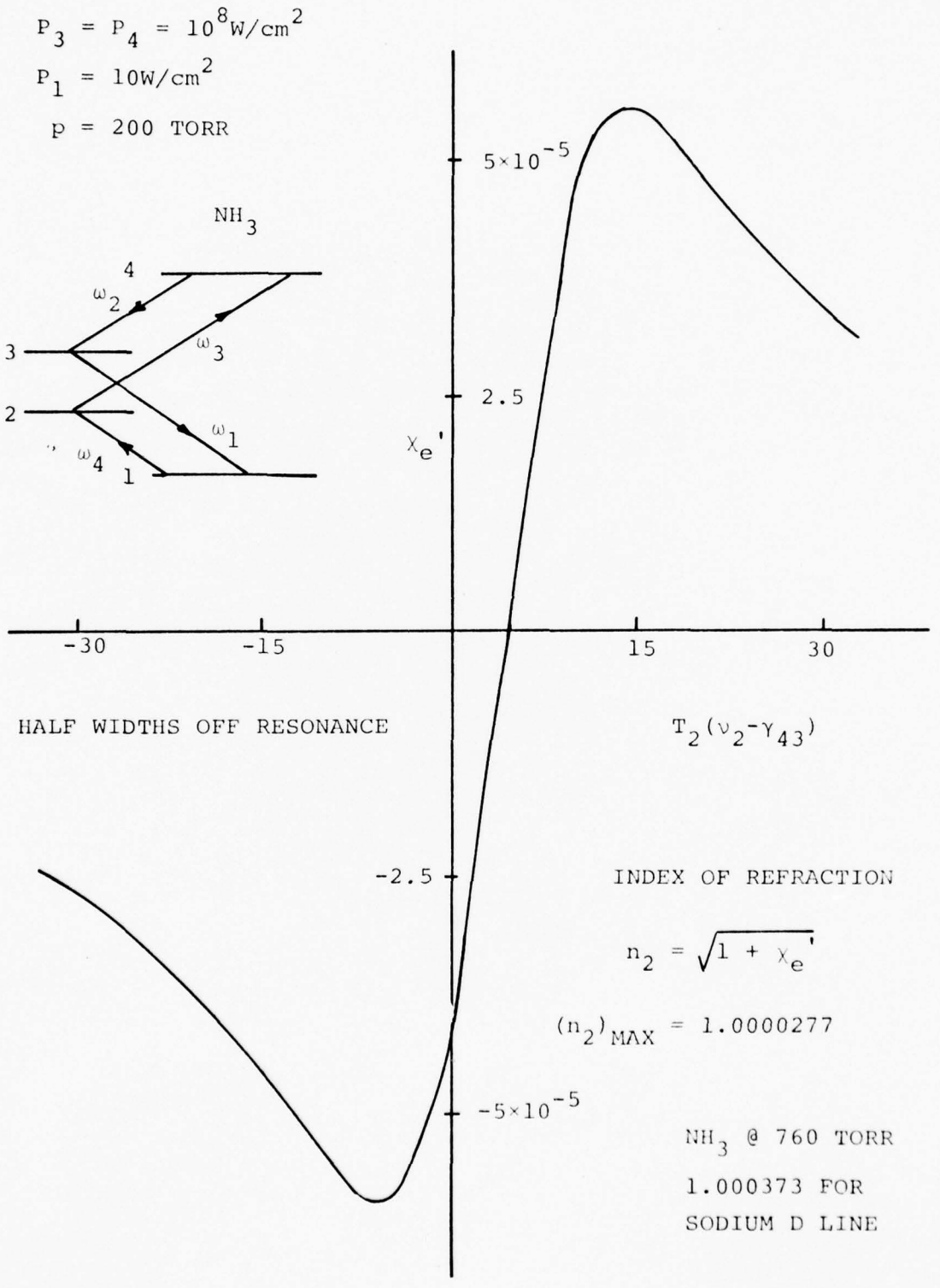

Figure 3. Electric susceptibility χ_e' at ω_2.

P_4, P_1 and the pressure P.

In spite of the pumps ω_3 and ω_4 being rather far off resonance, the linear plus Raman gains (as seen in Figure 1) at ω_2 reach a maximum value of 0.3 cm^{-1}. The parametric power generated at ω_2 for a one meter path length reaches a value of 3.79×10^{5} W/cm^2 (as seen in Figure 2) for a value of P_1 as low as 10 W/cm^2. Finally, as expected, χ_e' goes through zero where χ_e'' peaks (as seen from Figure 3) and attains a maximum value of 5.55×10^{-5} at 15 half widths off resonance.

Figures 4, 5, and 6 give a set of curves for lower pressure (p = 20 torr) and different parameters P_3, P_4 and P_1. An important point to be noted is that the peak gain at ω_2 has shifted from $\nu_2 > \gamma_{43}$ to $\nu_2 < \gamma_{43}$, i.e., the signal at ω_2 has been tuned.

In summary, a good approximate analytical solution to the four-wave four-level system has been obtained and an exact computer code for numerical analysis devised and applied to NH_3 with encouraging results.

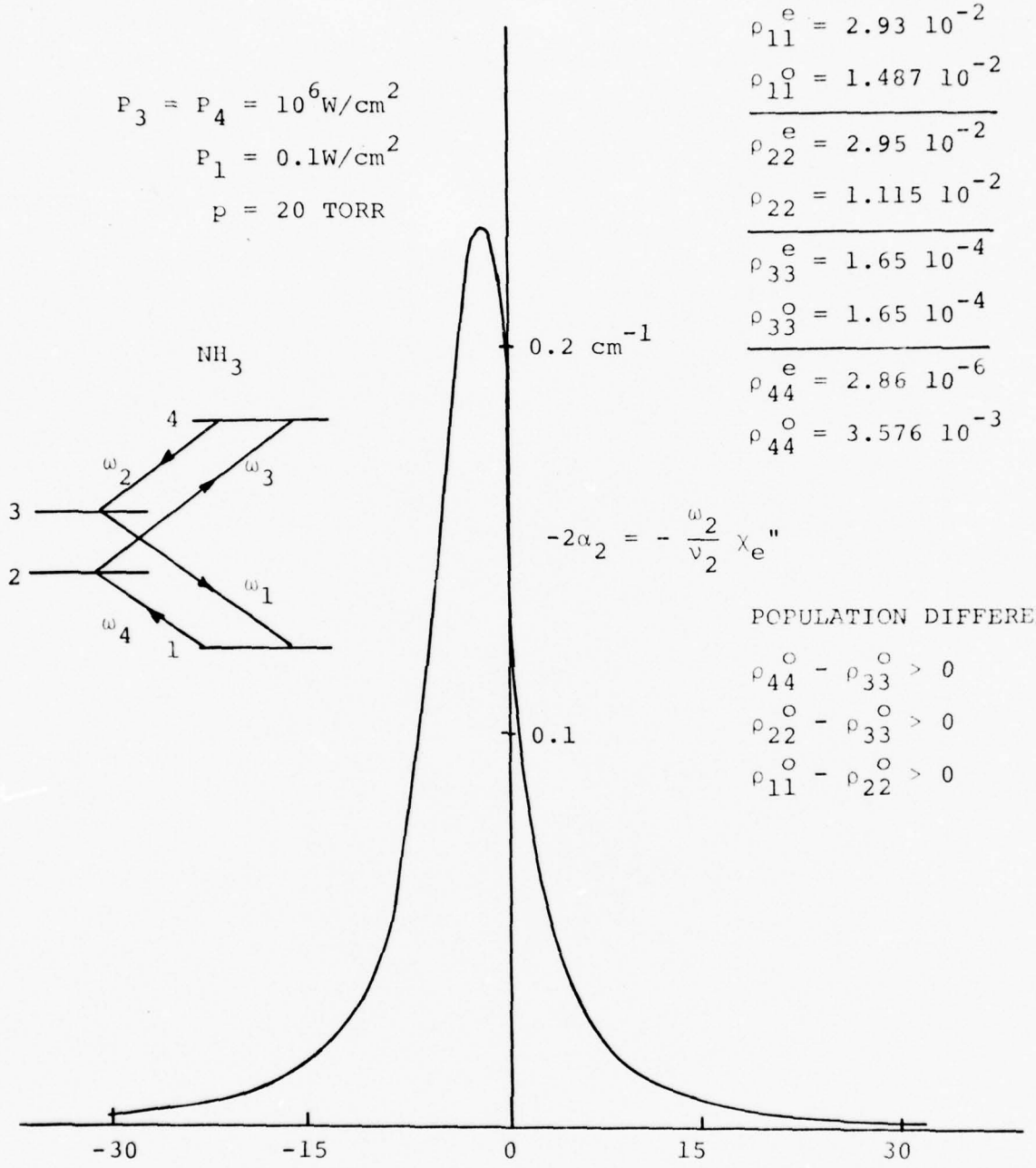

Figure 4. Linear plus Raman gain term $-2\alpha_2$ at ω_2.

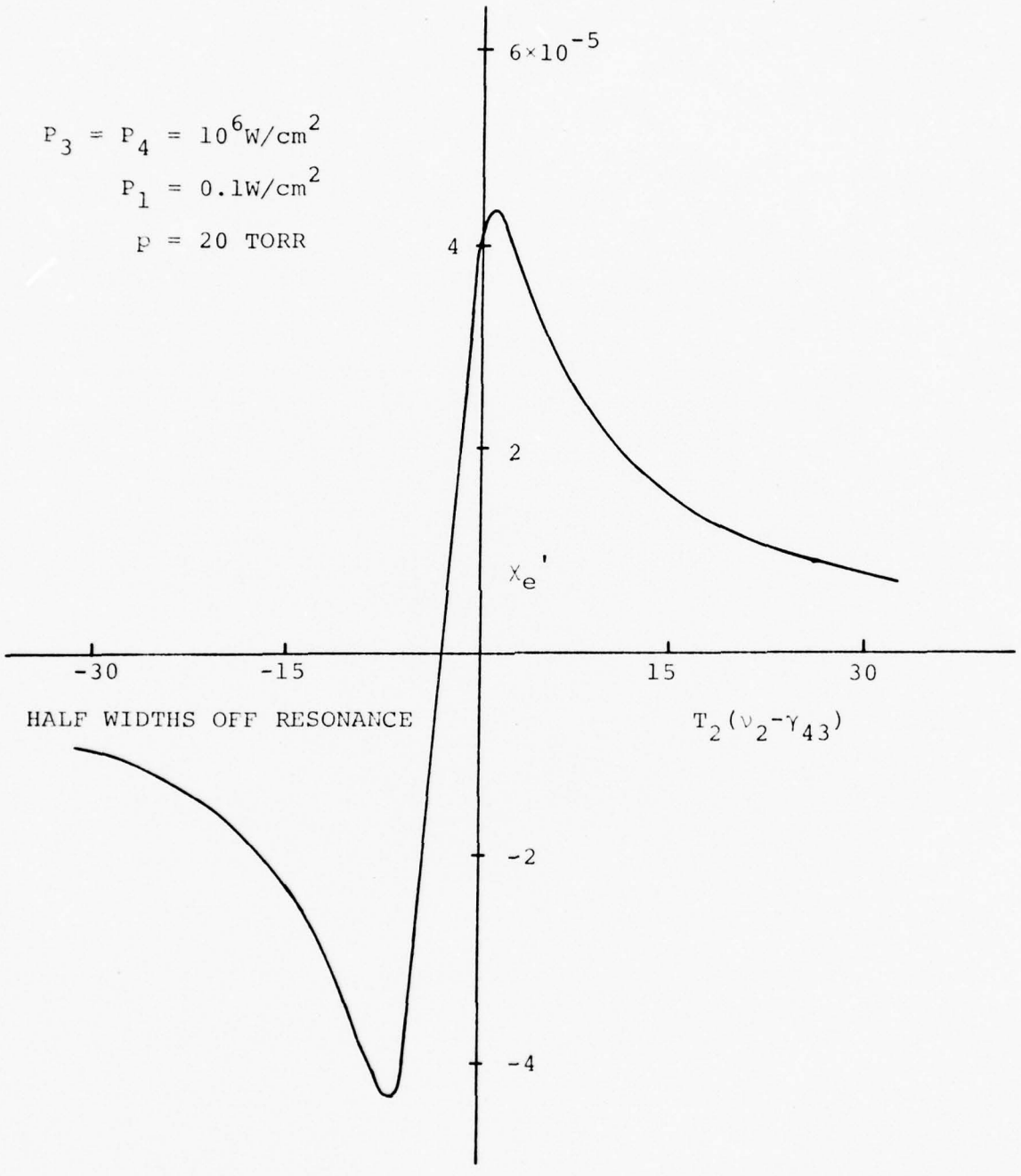

Figure 5. Electric susceptibility χ_e' at ω_2.

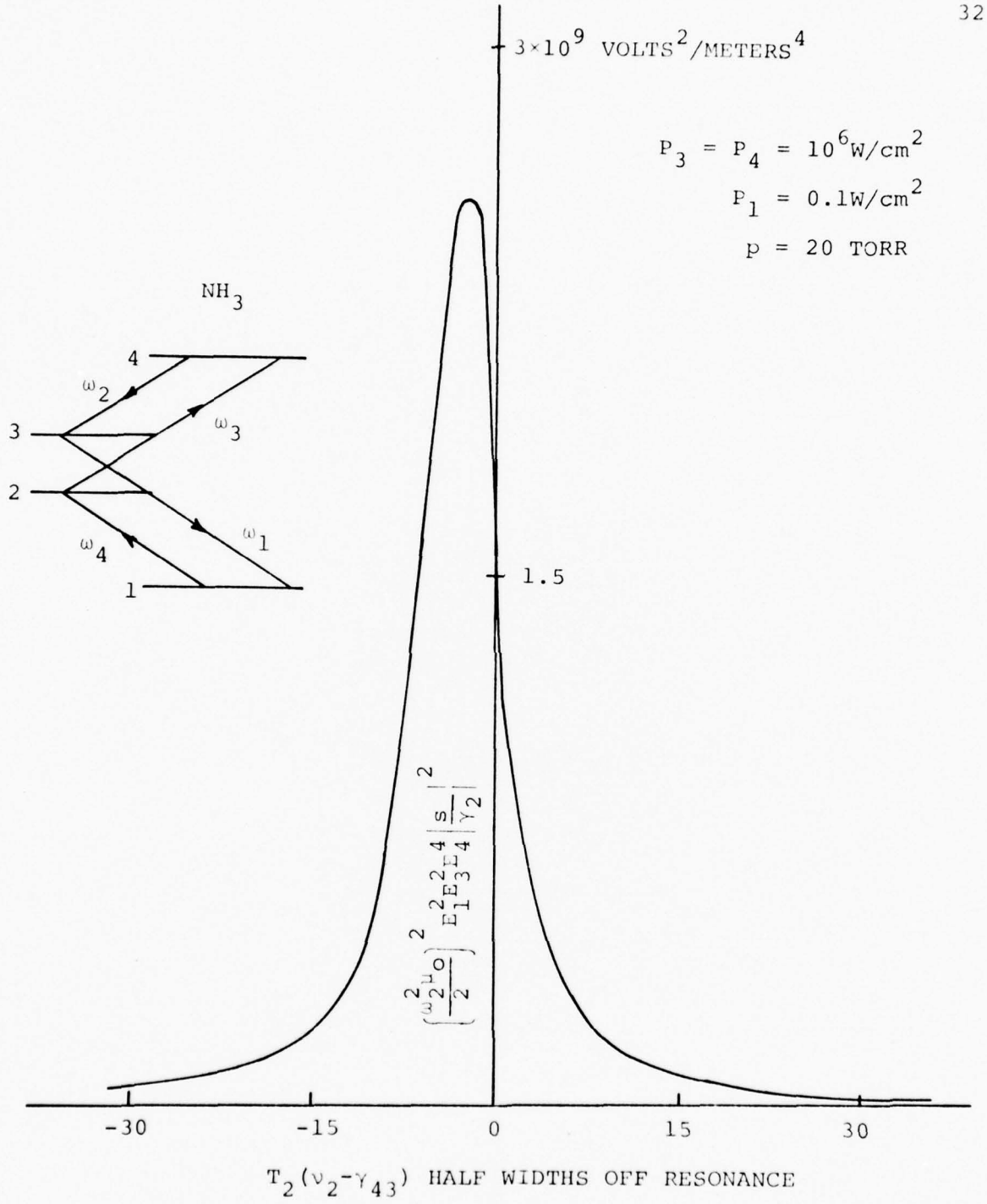

Figure 6. Parametric term associated with ω_2.

2.3 Optically Pumped NH_3 and PH_3 - E. Malk and E. Danielewicz

2.31 Introduction

Optical pumping of gaseous molecules has produced far infrared (FIR) emission on many discrete lines.[1] A simplified block diagram of an optical pumping experiment is shown in Figure 1.

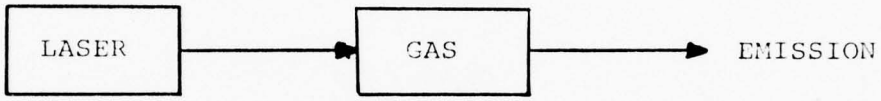

Figure 1. An optical pumping experiment.

To date, most optically pumped molecular laser experiments have been accomplished using a CO_2 laser on one of its 60 or so lasing transitions. The development of higher power CO_2 TEA (Transverse Excitation Atmospheric) lasers has produced multi-megawatt operation on many of its emission wavelengths. The higher pump power allows for a more versatile experiment.

Consider the energy level diagram shown in Figure 2. The laser frequency (ν_p) is "nearly resonant" with the transition frequency between levels 1 and 2. "Nearly resonant" depends on the pump power. For high pump power the frequency mismatch between the laser and the absorbing transition may be larger. The pumping efficiency (power absorbed/power incident) decreases, but population is transferred from level

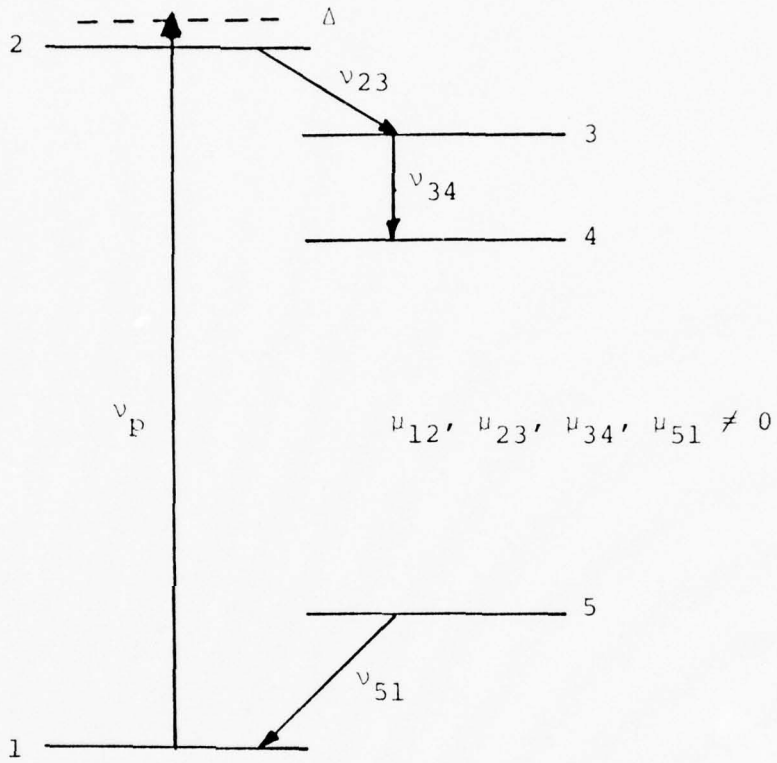

Figure 2. Typical energy level diagram for an optically pumped molecular laser experiment.

1 to level 2. Thus the TEA CO_2 laser because of its high power is a versatile pump laser.

Once non-equilibrium population is obtained in level 2, relaxation to equilibrium conditions begins. Optical and collisional relaxation mechanisms dominate the return to equilibrium. The optical relaxation is the desired result, and collisional relaxation is a competing process. Assume that the collisional relaxation rate is long compared to the optical rate. The attenuation at frequency ν_{ij} is described by Equation (1)

$$\alpha(\nu_{ij}) = \frac{c^2}{8\pi} \frac{A_{ji}}{\nu_{ij}^2} \left[N_j - \frac{g_j}{g_i} N_i\right] G(\nu_{ij}) \qquad (1)$$

A_{ji} = Einstein coefficient of transition

$G(\nu_{ij})$ = Line shape factor

C = Speed of light

g_i = degeneracy factor.

From this equation it may be seen that the attenuation can be negative (i.e., $\frac{g_i}{g_j} N_i > N_j$). This represents gain at ν_{ij}, the desired result. If the gain is larger than the loss, emission is observed.

Thus gain at ν_{23} and ν_{51} is expected if the above conditions are met. Following emission at ν_{23}, a similar condition may result between levels 3 and 4. This type of emission is called cascade emission.

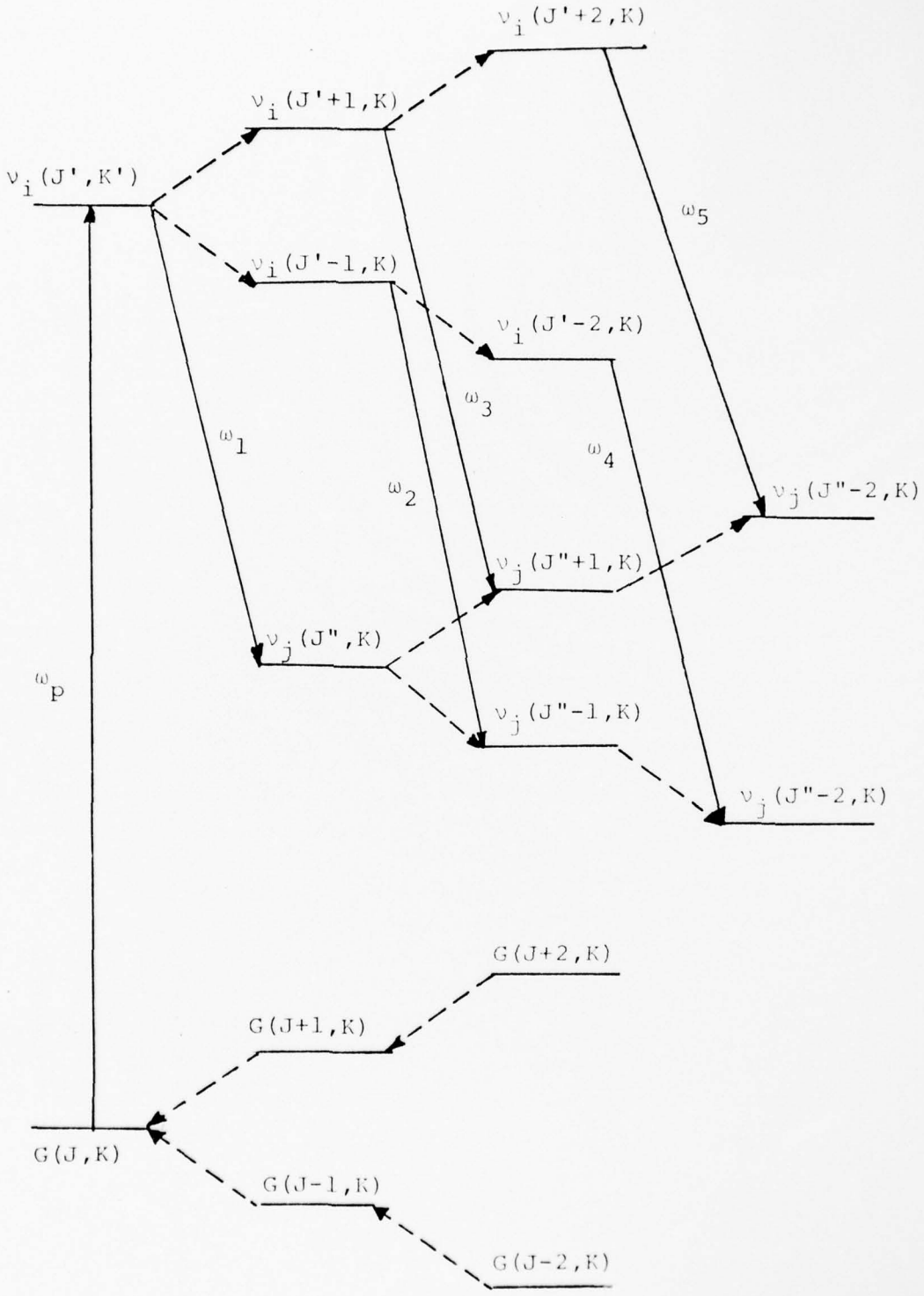

Figure 3. Multiple V-R emission energy level diagram.

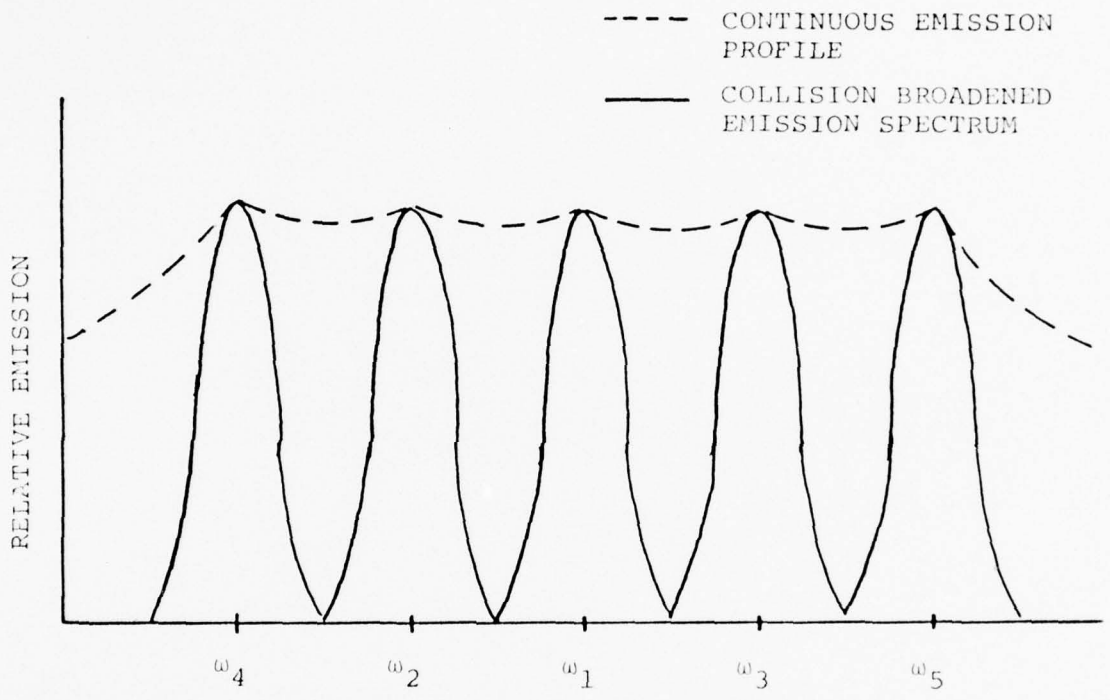

Figure 4. Emission spectrum of energy level diagram shown in Figure 3.

For real molecular systems, the ν_{12} transition is usually a Vibration-Rotation (V-R) transition with $\Delta v = +1$. The other transitions shown are usually pure rotation (R-R) transitions. The collisional relaxation mechanism is rotational relaxation and strongly dependent on gas pressure.

More recently emission frequencies have been obtained on V-R transitions. The collisional relaxation mechanism in this case, is vibrational (V-V) relaxation. V-V relaxation is usually slower than rotational relaxation, thus the pumping scheme shown in Figure 3 is possible. Entire vibrational manifolds may be population inverted in this manner, producing many emission lines near the same frequency. An emission spectrum may appear similar to the diagram shown in Figure 4. Collision broadening of the emission lines, should in principle, cause overlapping of the individual emission line gain curves. Significant overlapping will then produce a continuous emission profile through the emission spectrum. A frequency tunable source is therefore obtained. This technique has been used by Chang[2] to obtain laser action in CO_2 at 33 atmospheres of pressure.

2.32 Relevance

The utility of a tunable, coherent, narrow spectral line source in science and engineering is well known. Tunable signals are useful in evaluation of frequency characteristics

of devices, in studying resonance behavior, in high resolution spectroscopy, etc.

It is the purpose of this work to report progress in an attempt to obtain a frequency tunable laser. The results presented are only an intermediate step in the overall objective. The results do represent major steps toward obtaining an optically pumped tunable laser.

The following paragraphs present the sequence of events leading to and affecting the results presented. This demonstrates the interest of others in our work.

2.32.1 Sequence of Events

An optically pumped tunable laser was proposed[3] for study in Contract AFOSR 76-2988. An experimental apparatus was constructed and the investigation began. Several molecules were selected and experimentally tried, with negative results. T. Y. Chang and J. D. McGee[4] reported emission on a vibration-rotation transition at 12.812 μm optically pumped by CO_2. It was decided to repeat the experiment of Chang, and verify satisfactory operation of our experimental apparatus.

The Chang experiment was repeated successfully. The Gullberg, et al.[5] reference was consulted for additional possibilities. The possibilities were each tried. Infrared emission was observed by using two of the possibilities. The emission wavelengths were measured to be 12.08 μm (R(30) 9 μm

pump) and 11.46 μm (R(14) 10 μm pump).

Interest in the 12.08 μm line was very high because of the wavelength. ERDA is looking for a 12.15 μm laser for laser isotope separation (LIS).[6]

Prompted by the near coincidence of the achieved and the desired lines, a computer program to generate the transition frequencies was written. The program positively identified the 11.46, 12.08, and 12.812 μm transitions, with the correct pumping wavelengths. It was noted that all three lines behave parametrically in the same manner, that is: ${}^{a}_{s}R(J,K)$ absorption followed by ${}^{s}_{a}P(J+2,K)$ emission. The possibilities that were not observed did not fall into this scheme.

The gain of the 12.08 line appeared to be very large, (i.e., oscillation not critically dependent on cavity alignment). It was decided to try a 2 mm bore capillary tube to confine a high pump power density over a long path. The experiment, with the aid of John Leap, was set up.

Superfluorescent emission was observed on the 12.08 μm transition. Superfluorescent emission was not observed on either the 12.812 μm or 11.46 μm lines. The characteristics of the 12.08 μm line were studied in the capillary tube, and a paper was submitted to and accepted for publication in Applied Physics Letters.[7]

Peculiar behavior was observed for the 11.46 μm line. Calculation of population differences with pump saturation did

not result in a population inversion in the normal sense. The output of the 11.46 μm line was very much dependent on the input pulse shape. This is not typical of optically pumped lasers.

The off-resonance behavior of the 11.46 μm line was studied using an absorption technique. The results were peculiar and not easily understood.

During this time, D. Kim and J. Leap obtained superfluorescent emission on the 12.812 μm line in a 3 mm capillary tube. They also achieved higher output power on the 12.08 μm transition.

The inability to explain the 11.46 μm results prompted reinvestigation of the off-resonance behavior with greater control of experimental parameters. Further results indicated that the power of the input greatly affected the output of the 11.46 μm line. Pump power fluctuations caused the averaging techniques used to vary considerably from day to day. The only definite conclusion reached was that the 11.46 μm signal was off-resonance.

Some time later, we were contacted by S. M. Fry of Hughes Research Laboratories regarding our work with the 12.08 μm line. He reported[8] to us that he had achieved multi-line laser operation from the same transition, by pumping NH_3 with N_2 as a buffer gas at pressures up to one atmosphere. Subsequently, D. Kim used a similar technique in a capillary tube

to generate many of the same lines observed by Fry. D. Kim[9] also discovered a new line at 12.28 μm by pumping with the $P(32)_{10}$ CO_2 transition.

T. Y. Chang and J. D. McGee report "off-resonant infrared laser action in NH_3 and C_2H_4 without population inversion". Our observed lines and D. Kim's 12.28 μm lines are included in his study. The results of his experiment concur with ours, but we believe his explanation to be suspect.

2.33 Experimental Results

Superfluorescent emission at 12.079 μm has been observed for the first time by pumping the sR(5,0) transition of the ν_2 fundamental band of $^{14}NH_3$ with the R(30)(9.217 μm) transition of a CO_2 TEA laser. Over 2 kW of pulsed output power was obtained in a single pass, using a mirrorless capillary tube waveguide geometry. The laser transition has been identified as the sP(7,0) transition from the ν_2 vibrational band to the ground state. Another new line at 11.460 μm was observed with the R(14)(10.286 μm) line pumping the aR(1,1) transition in the cavity configuration. The 11.460 μm line has been identified as the aP(3,1) transition. In addition, pumping the aR(6,0) transition with R(16)(9.294 μm) line produces emission at 12.812 μm as previously observed by Chang and McGee.[4] The results of the experimental investigation are summarized in Table I. Subsequent to the publication of these results,[7] S. M. Fry[8] has reported obtaining 41 additional transitions by pumping the sR(5,K) levels with R(30)(9.217 μm) CO_2 line by pressure broadening the absorbing transition. These emission lines are obtained in a cavity. K. J. Kim[9] has obtained superfluorescent emission in a manner similar to that of Fry, as well as some new transitions.

A detailed examination of the experimental data obtained for the 12.079 μm and 11.460 μm transition follows the description of the experimental apparatus.

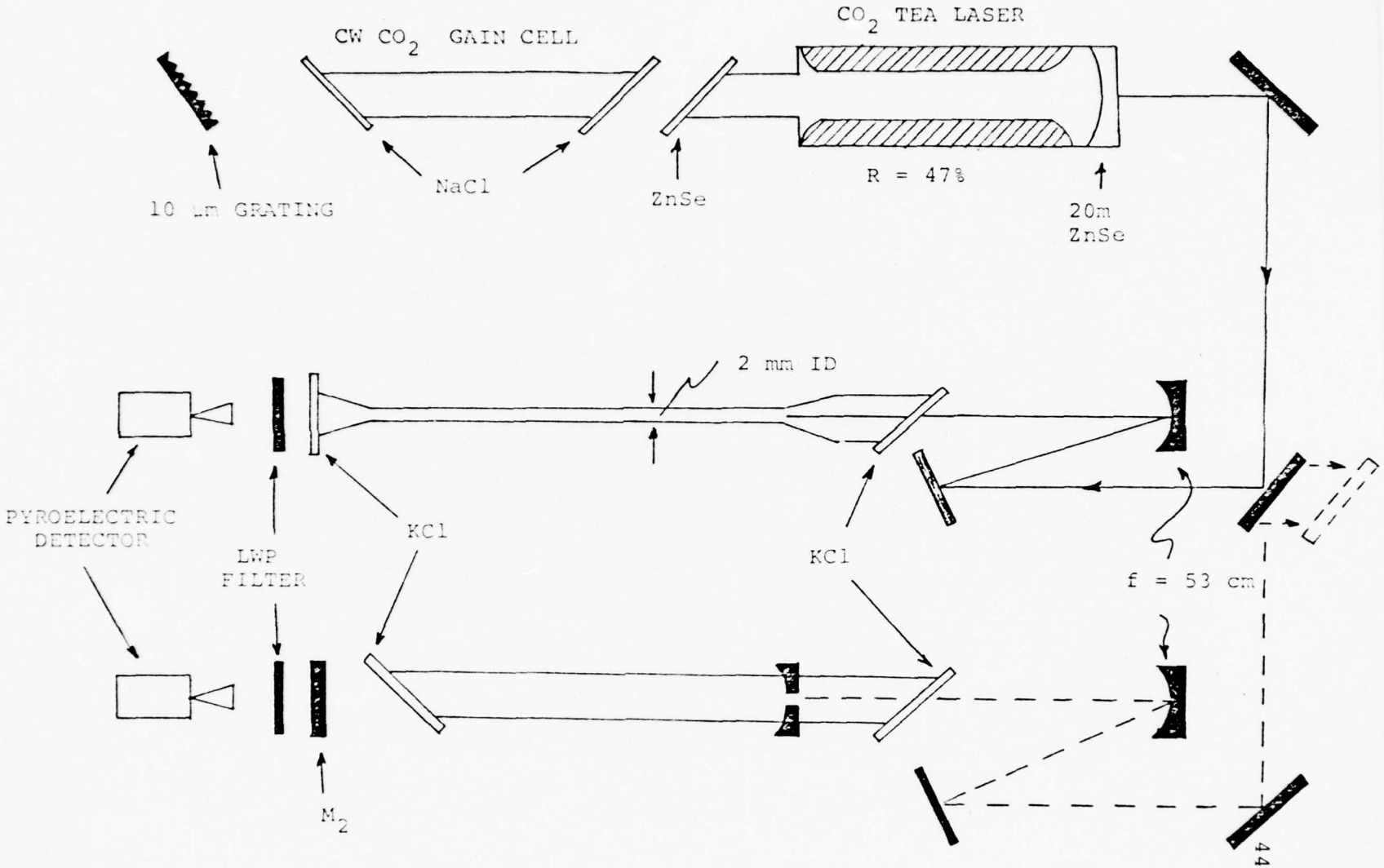

Figure 5. Schematic diagram of the experimental set-up.

2.34 Experimental Configuration

The experimental configuration used in generation of the infrared transitions of NH_3 is shown in Figure 5.

The grating-tuned atmospheric-pressure CO_2 (TEA) laser emitted up to 1.2 MW peak power on R(30) 9.217 μm transition in a 160 nsec (FWHM) pulse. The laser was operated with a 10:1:50 mixture of CO_2:N_2:He to obtain a pulse with a minimum nitrogen tail. A CW CO_2 gain cell was also used in the TEA laser cavity to suppress the normal self-mode-locking of the TEA laser and to force the laser to oscillate on a single longitudinal mode near line center.[11] The NH_3 was contained in a semi-confocal cavity with internal gold coated mirrors. The input mirror had a 4m radius of curvature with a 2.0 mm dia. coupling hole. The output mirror was a flat mirror with a 0.5 mm hole mounted in a translatable stage for longitudinal cavity tuning. The CO_2 pump radiation was focused into this cavity with a 0.53m focal length mirror. It was found that the gain bandwidth of the lines was sufficiently high such that cavity tuning was unnecessary. An external dielectric mirror with 8.0% transmission at 12.079 μm and a KCl Brewster window parallel to the pump polarization could then be substituted for the output mirror.

To increase the pump laser confinement, a 1 m long 2 mm fore Pyrex capillary tube was substituted for the open resonator cavity described above. A KCl Brewster window was used

as the entrance window and another KCl window normal to the tube was used at the output end. Aside from the Fresnel reflection from the output window there was no intentional feedback in the apparatus and the effects of unwanted regeneration were minimal. Focusing the CO_2 pump produced a power density of $\sim$ 26 MW/cm^2 inside the dielectric guide.

The output of either configuration was analyzed with a Heath 1/3 meter grating monochromator using the CO_2 lines observed in first order for accurate calibration.

Pressures were measured with a M.K.S. Baratron gauge with range from 0-10 torr.

Table 1. Calculated Absorption (ν_a) and Emission (ν_e) Transition Frequencies of NH_3. The offset of the CO_2 pump frequency (ν_p) from the absorption line is $\Delta\nu = \nu_a - \nu_p$. The accuracy of the calculated emission wavelengths is estimated as ±.0005 μm.

CO_2 PUMP	R(30)	R(14)	R(16)
ν_p(CM-1)	1084.635	971.930	1075.988
NH_3 ABS. TRANS.	sR(5,0)	aR(1,1)	aR(6,0)
ν_a(CM-1)	1084.628	971.881	1076.028
$\Delta\nu$(GHz)	-0.20	-1.47	+1.20
NH_3 EM. LINE	sP(7,0)	aP(3,1)	aP(8,0)
ν_2(CM-1)	827.876	872.565	780.556
λ_e (μm)	12.0791	11.4605	12.8115

2.35 The 12.08 μm Transition

The most important feature of the 12.08 μm transition is its superfluorescent behavior. The data taken will reflect this fact.

A partial energy level diagram is shown in Figure 6. Shown in the figure are the FIR emission lines that have been previously observed. The 12.08 μm transition is also shown. The dashed transition has not been observed. This line should be observed as a cascade transition following emission at 12.08 μm. No detailed search was made to observe this 72.4 μm line. This cascading line may contribute significantly to the pressure-pulse time behavior to be discussed later in greater detail.

The frequency mismatch of the absorbing transition and the CO_2 pump line may easily be calculated from the diagram. The mismatch is -0.2 GHz.[12] Experimentally measured values using infrared-microwave double resonance are not available because the antisymmetric (7,0) ground state level does not exist. This near resonance condition partially explains the large number of cascading transitions that are observed, (i.e., large absorption coefficient).

The dipole selection rules for transitions involving energy levels with K = 0, preclude the possibility of pure inversion ($\Delta J = 0$) transitions. To a first approximation, rotational relaxation obeys the dipole selection rules.

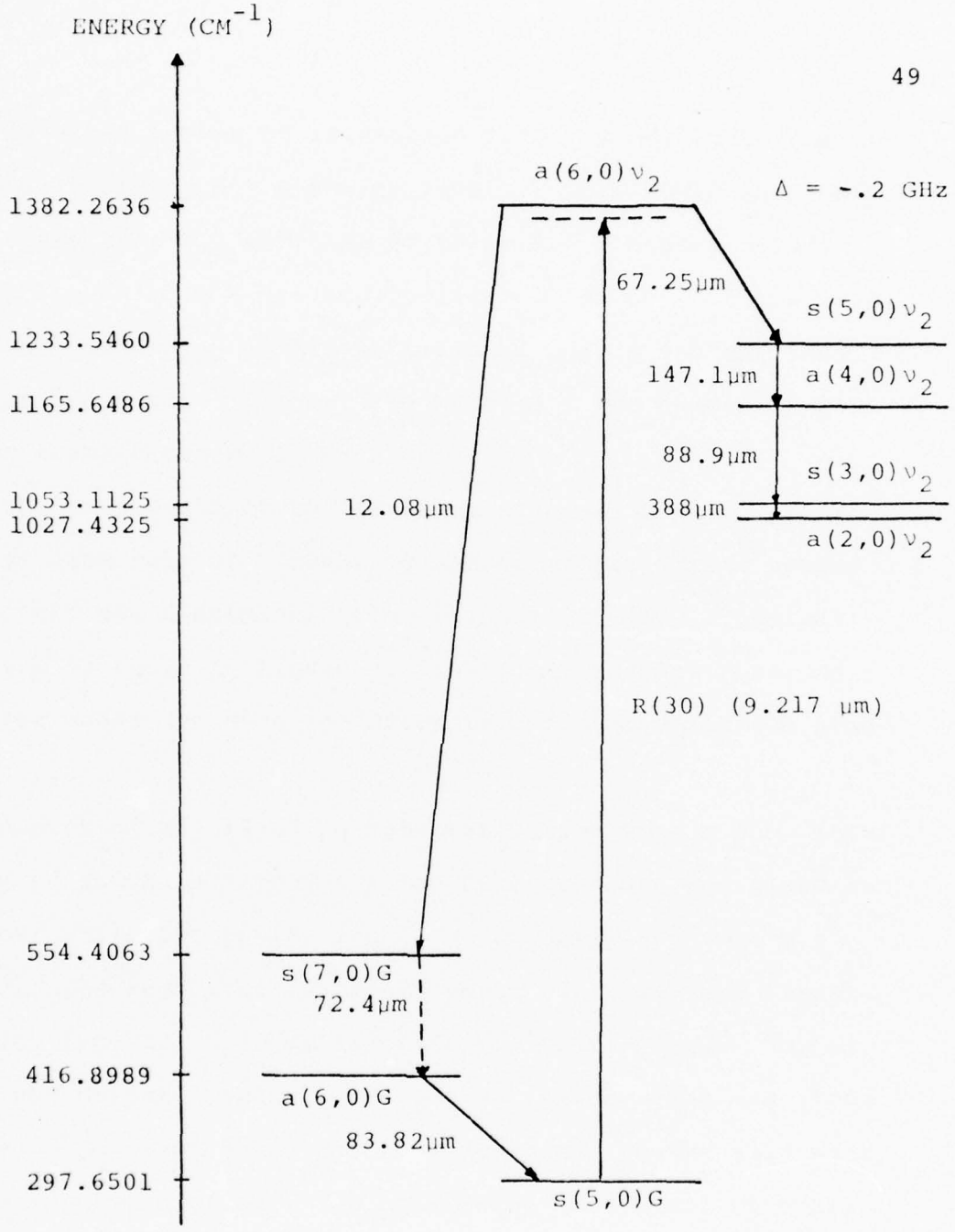

Figure 6. NH_3 energy level diagram for the 12.08 μm emission line.

Therefore the number of relaxation paths is decreased for systems involving K = 0 energy levels. This would lead one to believe that the lifetime of these K = 0 energy levels may be longer than $K \neq 0$ energy levels. If this is the case, then the stimulated radiative lifetime may be shorter than the excited state lifetime, and hence a large number of cascading transitions would be likely.

The wavelength of the 12.08 μm line was determined from several data runs of a scanning spectrometer. The measured wavelength was determined to be 12.08 ±.008 μm. A typical data run is shown in Figure 7. The CO_2 lines are observed in first order and used for accurate calibration of the spectrometer.

A plot of the 12.08 μm detector output versus pump input energy is shown in Figure 8. The cell pressure was fixed at 5.0 torr while the energy input to the capillary tube was varied. The resulting 12.08 μm output exhibits very linear behavior from 20 to 40 millijoules of input energy. Beyond 40 mJ the output appears to become saturated. The magnitude of the output signal was strongly dependent on the alignment of the input radiation. The case shown is typical of near optimum alignment of the input radiation. This alignment is easily achieved by maximizing the transmission of the input radiation through the capillary.

Two plots of normalized output signal at 12.08 μm versus

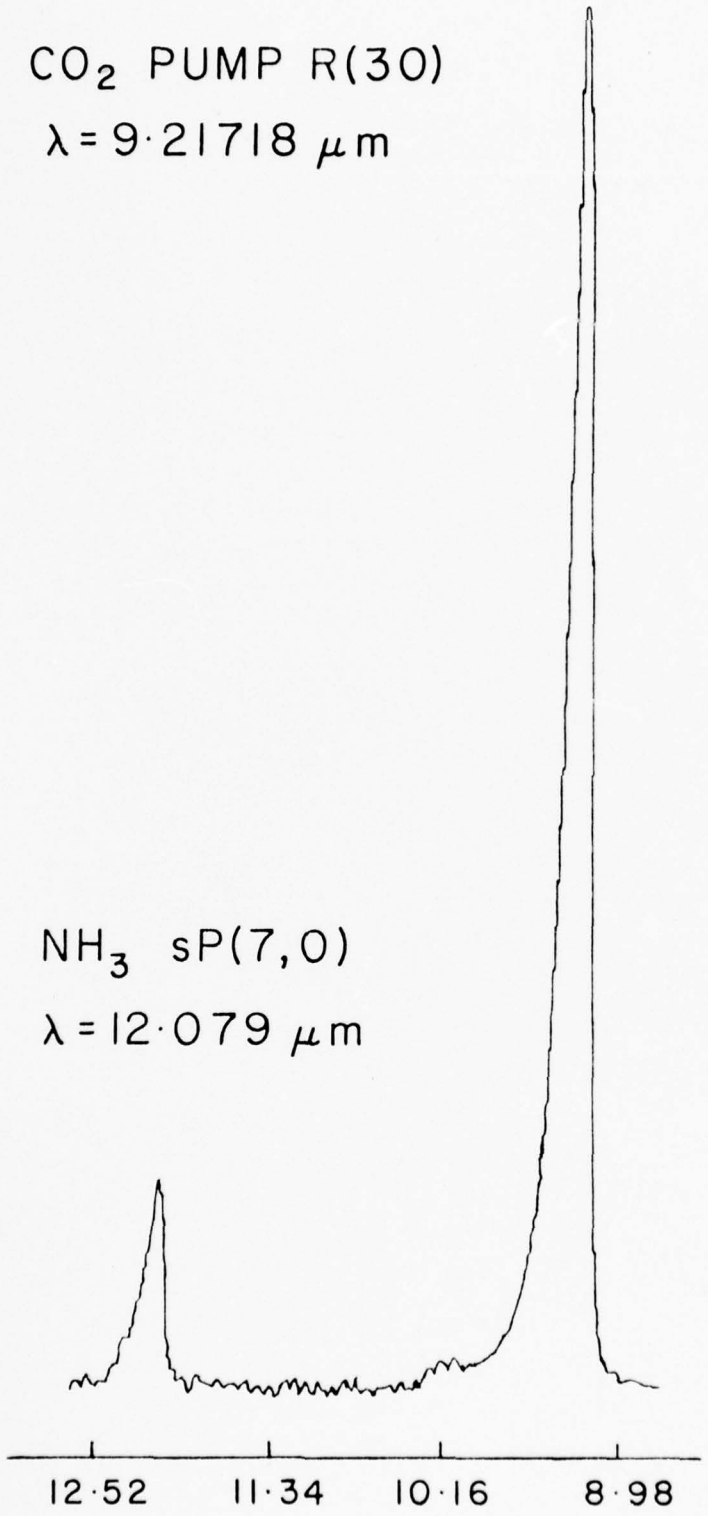

Figure 7. Wavelength scan showing 12.08 μm and 9.217 μm lines.

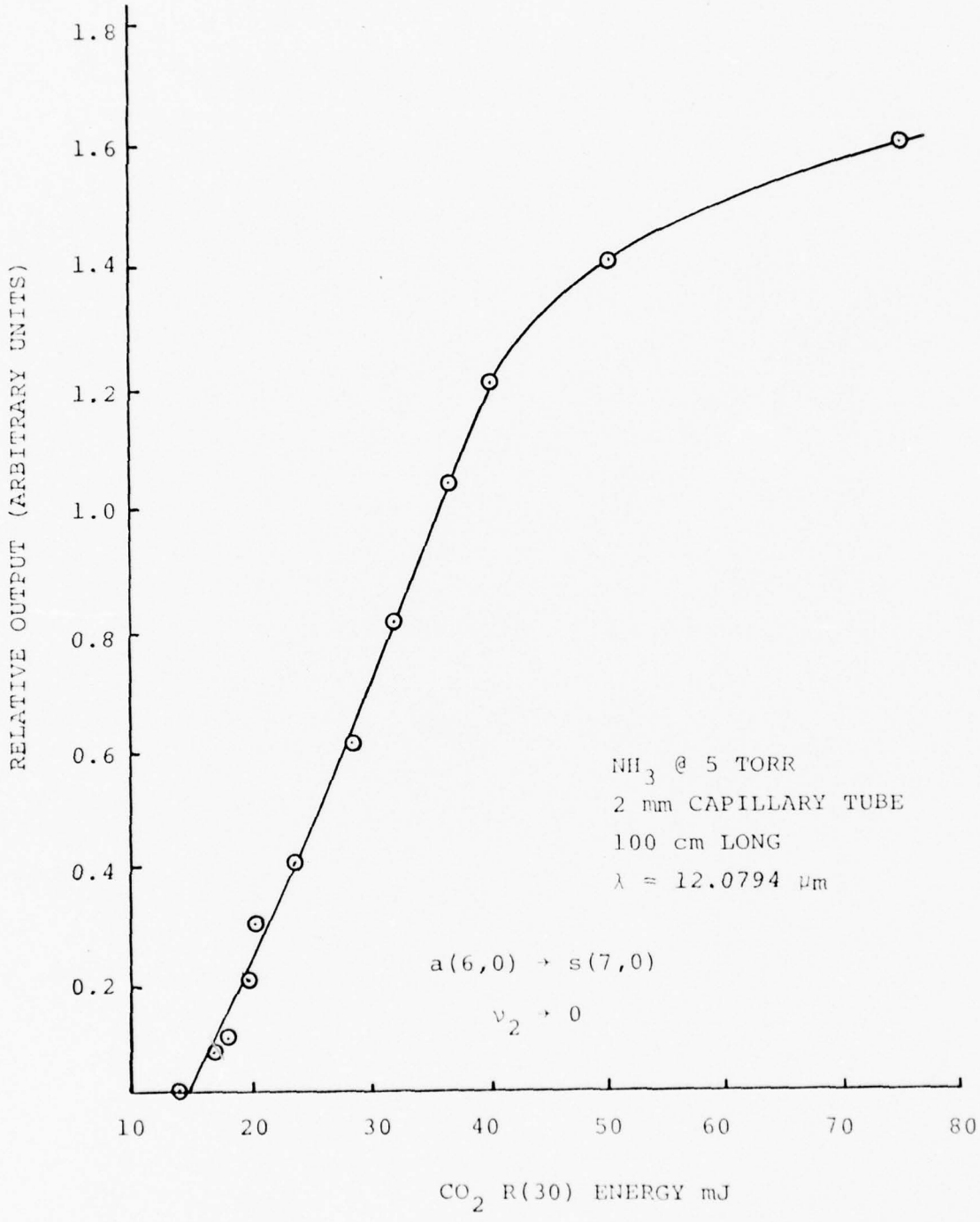

Figure 8. 12.08 μm output vs. CO_2 input energy.

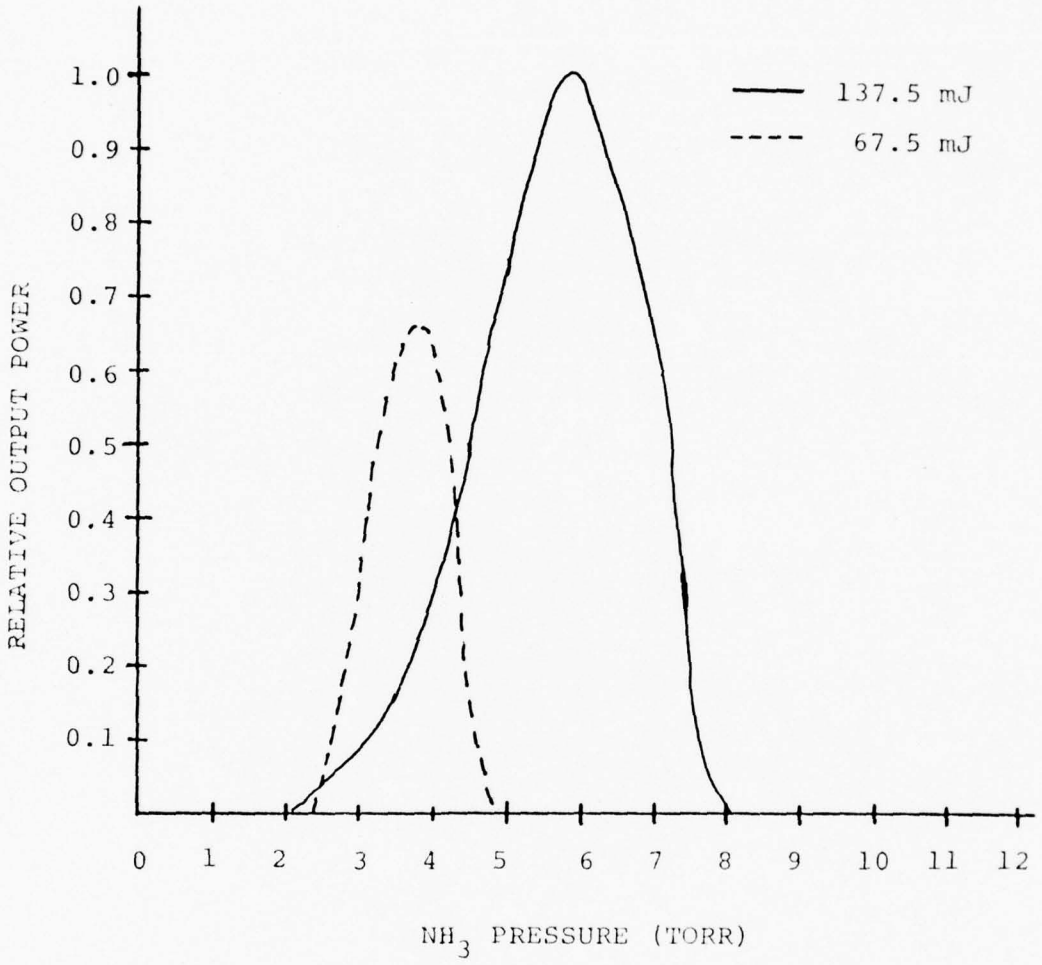

Figure 9. 12.08 μm output power vs. cell pressure of NH_3.

cell pressure are shown in Figure 9. Input energies of 67.5 and 137.5 mJ are used. The two plots show that the optimum pressure and signal strength increase with increasing input power. Additional data is required to determine if saturation is being observed.

The formation of "self-focusing" type streamers was observed during propagation of the R(30) CO_2 transition through a non-capillary type tube. This effect was observed for higher pump intensities with cell pressures near the optimum 12.08 μm output signal pressures. This "self-focusing" type behavior may do much to improve the output of the 12.08 μm line.

The additional focusing may cause local field strengths to increase immensely. The reduced propagation spotsize of the pumping radiation may cause attenuation losses of the capillary to become smaller. Prior to Chang's latest paper,[10] it was believed that this "self-focusing" effect may have kept him from observing the 12.08 μm line. Chang's experimental pumping cell is pumped off axis. This feature, plus self-focusing led us to believe that the actual gain region would be very small. Our experiment is axially pumped, hence self-focusing occurs on axis.

The most interesting, and least understood, data taken contain information on the output pulse time behavior as a function of cell pressure. Chang observed similar behavior

for the 12.812 μm transition. The output pulse-width and structure show very strong dependence on the cell pressure. Chang[4] attributed this behavior to rotational relaxation rates that vary with pressure. The effects of the FIR emission lines, which occur at lower pressures, on the 12.08 and 12.812 μm lines have not been studied. These effects are believed to contribute to the behavior observed. A detailed study of the problem by looking at the FIR emission lines would shed much light on this effect.

A series of scope traces have been reproduced in Figure 10. These demonstrate the cell pressure-pulse-width and structure effect just described. These pictures were taken using a Cu:Ge detector. Figure 10 shows a typical pump laser pulse as detected by a Ge photon drag detector. The response time of such a detector is in the subnanosecond region. This trace shows that the pump laser is operating on a single longitudinal mode, and the lack of Nitrogen tail because of the CO_2:N_2:He mix used.

The remaining traces are all for the 12.08 μm emission line. Figure 10b is the only picture of the output with a feedback cavity being used. The trace shows typical output operating at the optimum pressure, 2 torr, in this case.

Traces 10c through 10h show a sequence of traces obtained while the cell pressure is being lowered. Traces 10c through 10e show the pulse-width lengthening as the pressure

(a) CO_2 TEA LASER

PHOTON DRAG DET.

R(30) - 9.6 μm

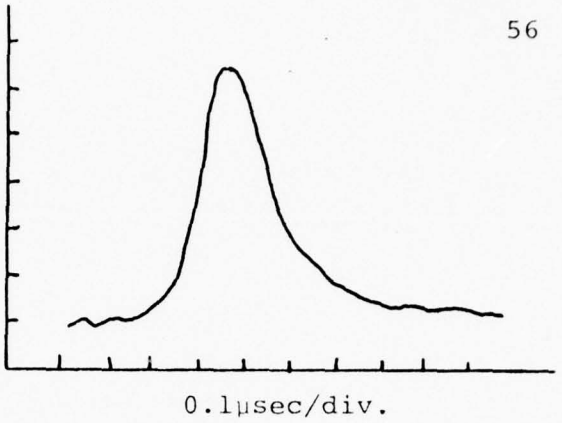

(b) p = 2 TORR NH_3

λ = 12.079 μm

Cu:Ge DET.

LP FILTER

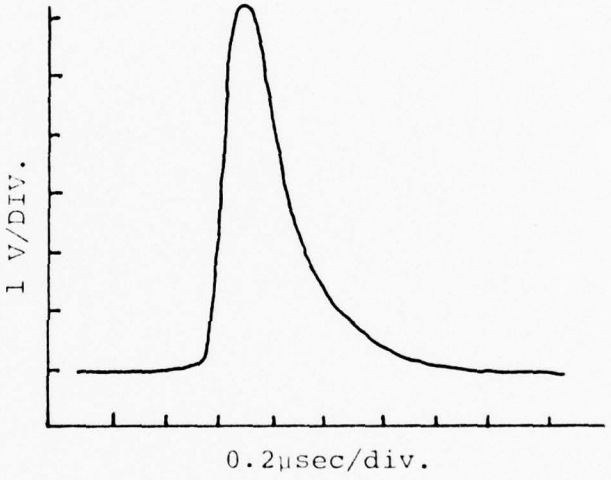

(c) p = 5.3 TORR NH_3

λ = 12.0794 μm

R(30) 9.6 μm PUMP

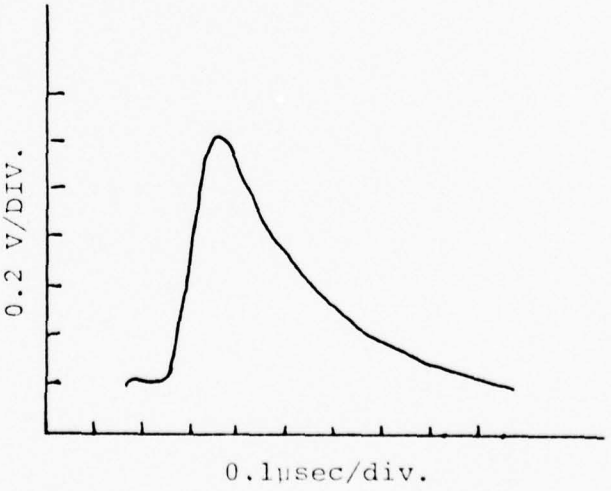

Figure 10. Scope traces of 12.0794 μm NH_3 signal for various pressures.

(d) p = 2.0 TORR NH_3

λ = 12.0794 μm

Cu:Ge DET.

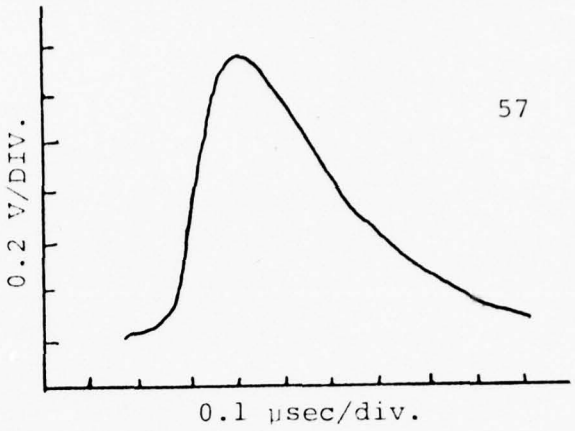

(e) p = 1.0 TORR NH_3

λ = 12.0794 μm

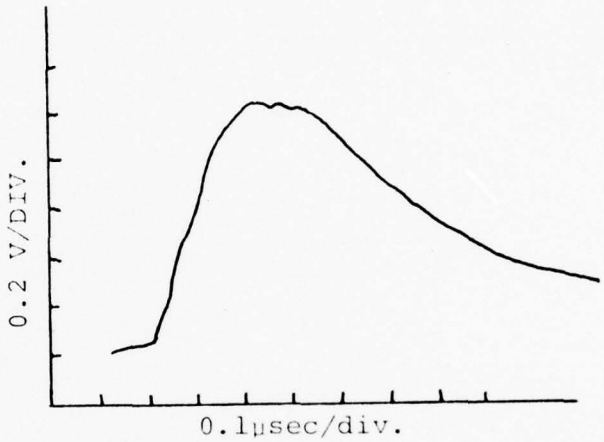

(f) p = 0.2 TORR NH_3

λ = 12.0794 μm

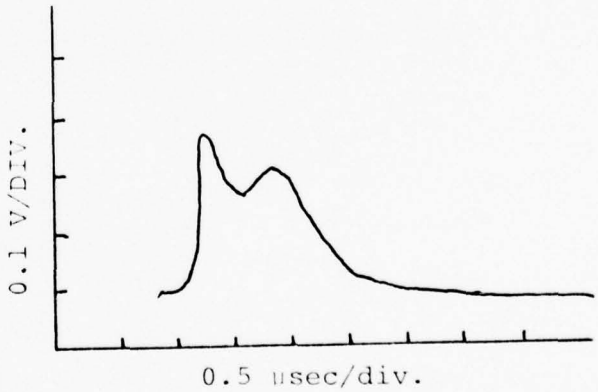

Figure 10. Scope traces of 12.0794 μm NH_3 signal for various pressures.

(g) p < 0.1 TORR NH_3

Cu:Ge DET.

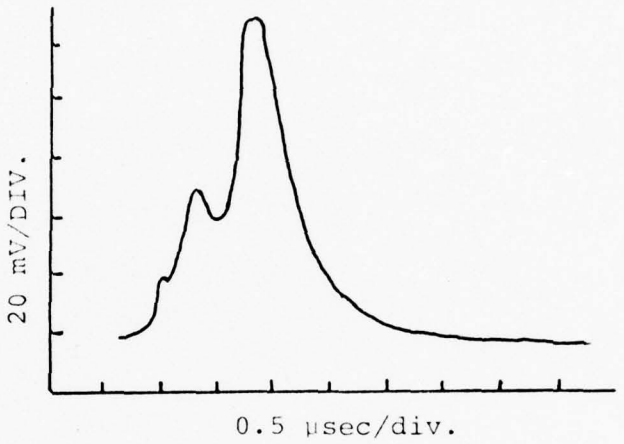

(h) p ≈ 0 TORR NH_3

R(30) - 9.6 μm

PUMP

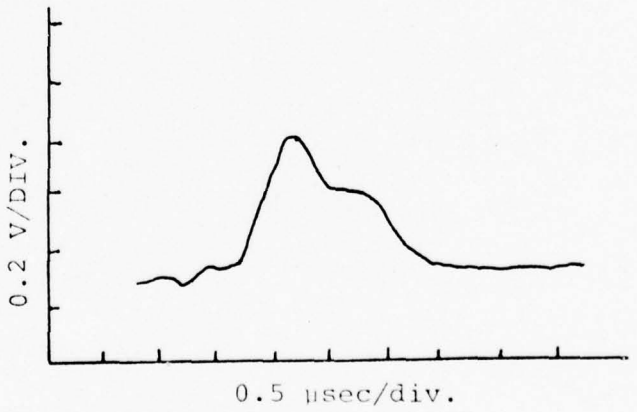

Figure 10. Scope traces of 12.0794 μm NH_3 signal for various pressures.

is decreased. A little structure begins to appear at a cell pressure of one torr. Decreasing the pressure even further produces pronounced structure as is observed in the remaining traces. A time resolved frequency study should be accomplished for a better understanding of this data. Study of the FIR emission lines may prove that competition processes will explain this behavior.

In summary of the presentation of the 12.08 μm results, a table of typical operation characteristics and pertinent spectroscopic information is given.

Table 2. Summary of 12.08 μm Data.

SPECTROSCOPIC SUMMARY

EMISSION FREQUENCY AND WAVELENGTH	827.876 cm^{-1}	12.079 μm
EMITTING TRANSITION	sP(7,0)	
ABSORBING TRANSITION AND FREQUENCY	sR(5,0)	1084.628cm^{-1}
CO_2 PUMP TRANSITION AND FREQUENCY	R(30)	1084.635cm^{-1}
PUMP MISMATCH	-.20 GHz	-.007 cm^{-1}

TYPICAL OPERATING CHARACTERISTICS

CO_2 TEA LASER

MIXTURE	10:1:50	CO_2:N_2:He
POWER	1.2 MW	
PULSE LENGTH	160 nsec FWHM	
MODE CHARACTER		
LONGITUDINAL	SINGLE MODE	
TRANSVERSE	LOWER ORDER	

NH_3 12.08 μm EMISSION

CAVITY CONFIGURATION

CAVITY LENGTH	1.3 m
OPTIMUM PRESSURE	∿ 2.0 TORR
OUTPUT POWER	∿ 1 kW
PULSE LENGTH	DEPENDS ON PRESSURE

Table 2. Summary of 12.08 μm Data.

CAPILLARY CONFIGURATION		
CAPILLARY LENGTH AND BORE	1 m	2 mm
OPTIMUM PRESSURE	∿ 4.8 TORR	
OUTPUT POWER	∿ 2 kW	
PULSE LENGTH	DEPENDS ON PRESSURE	
CONVERSION EFFICIENCY	.33%	

2.36 The 11.46 μm Transition

The distinguishing feature of the 11.46 μm emission line is that emission occurs in the absence of a population inversion. This type of character is true for a stimulated Raman emission line. A Raman emission line is tunable, by tuning the pumping radiation. This tunable feature is desirable for many reasons and makes this emission line important.

A partial energy level diagram is shown in Figure 11. The transition structure is similar to the 12.08 μm figure. The pumping transition is considerably further from resonance in this case. A pump detuning of 1.445 GHz has been measured by Oka[12] using infrared-microwave double resonance techniques. Two far IR transitions have been observed in conjunction with this pumping transition. The 281.27 μm transition is observed as a cascade transition following relaxation (or emission) from the $s\nu_2(2,1)$ level to the $a\nu_2(1,1)$ level. The transition wavelength is 2.13 mm and is not observed. The other FIR transition occurs at 256.7 μm. It results from a cascade into the level being pumped (Ga(1,1) level) from the Gs(2,1) level. Gullberg, et al.[5] noted that this transition exhibited little polarization discrimination and attributed this fact to a long relaxation time for filling the depleted lower level. Also noted for the 281.27 μm transition, the emission was sensitive to longitudinal tuning of the pump radiation.

The dashed transition at 165 μm and a microwave transition

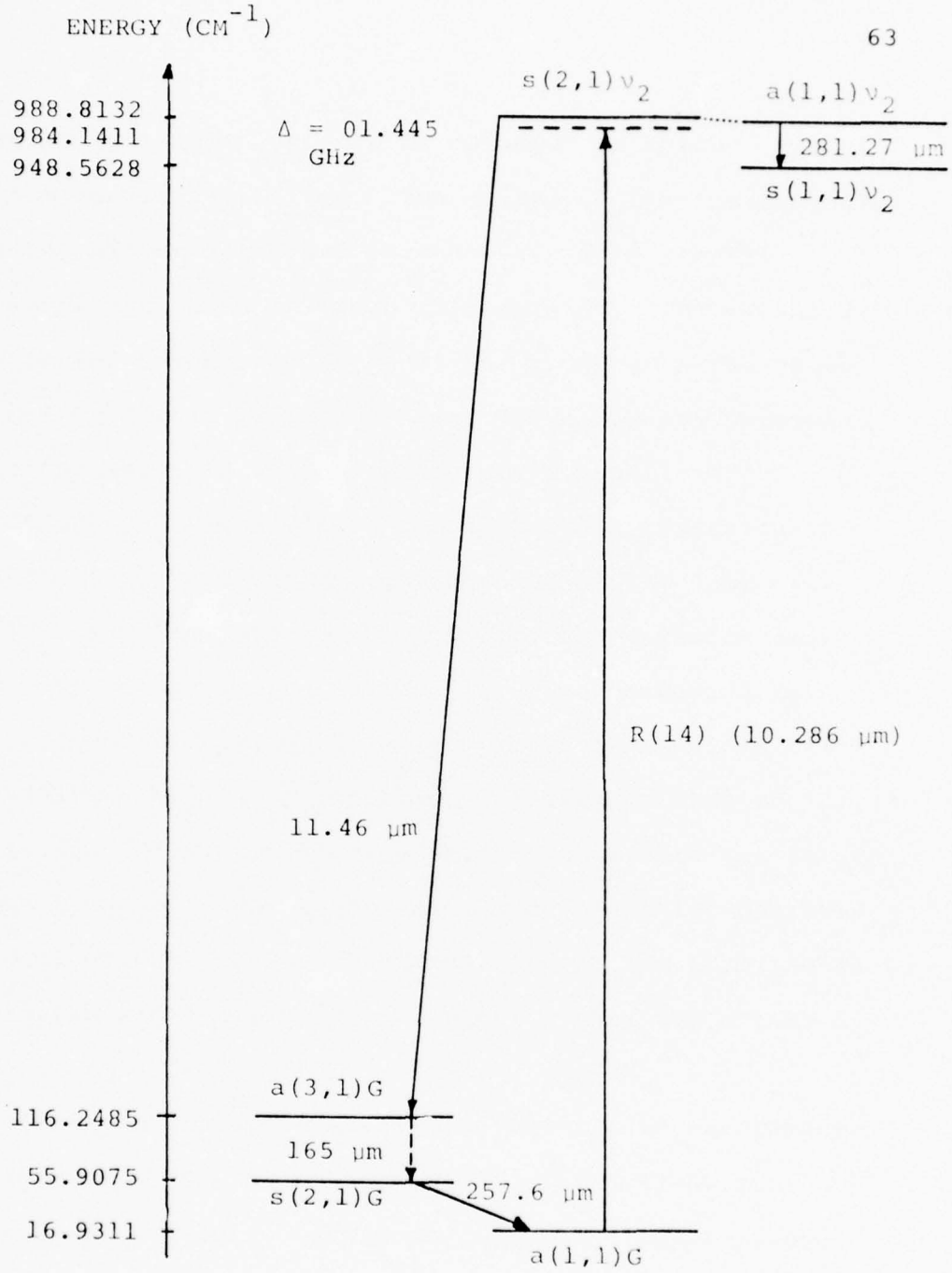

Figure 11. NH_3 energy level diagram for the 11.46 μm emission line.

at 13.48 mm (not shown) should be observed as cascade transitions from the 11.46 μm line. The microwave line is expected to have the higher gain, and is therefore more likely.

A wavelength scan is shown in Figure 12. The measured wavelength was determined to be 11.463 ±.008 μm. The value determined by Curtis is 11.4605 μm. The agreement between measured and assigned values is therefore excellent.

Difficulty in measuring the output characteristics of the 11.46 μm line was encountered because of the lack of a good filter to discriminate the pump and the emission wavelengths. The transmission of the filter was measured to be on the order of .1% at 10.286 μm and about 3% at 11.46 μm. The transmitted CO_2 10 μm radiation was greater than the 11.46 μm transition emission. Studies were accomplished through the Heath spectrometer. For this reason good operating characteristics data are not given. The signal is weaker than the 12.08 μm transition and operates from 0.5 → 1.8 torr for a 1 MW input.

The feature mentioned earlier of particular importance is the lack of a population inversion. This may be shown by examining the partioning of the population at equilibrium.

The partition function for the population is given by Equation (2)

$$f_{JK} = \frac{S(I,K)(2J+1)}{4I^2 + 4I + 1} \quad \frac{B^2C}{\pi(kT)^3} \exp(-E_{JK}/kT) \qquad (2)$$

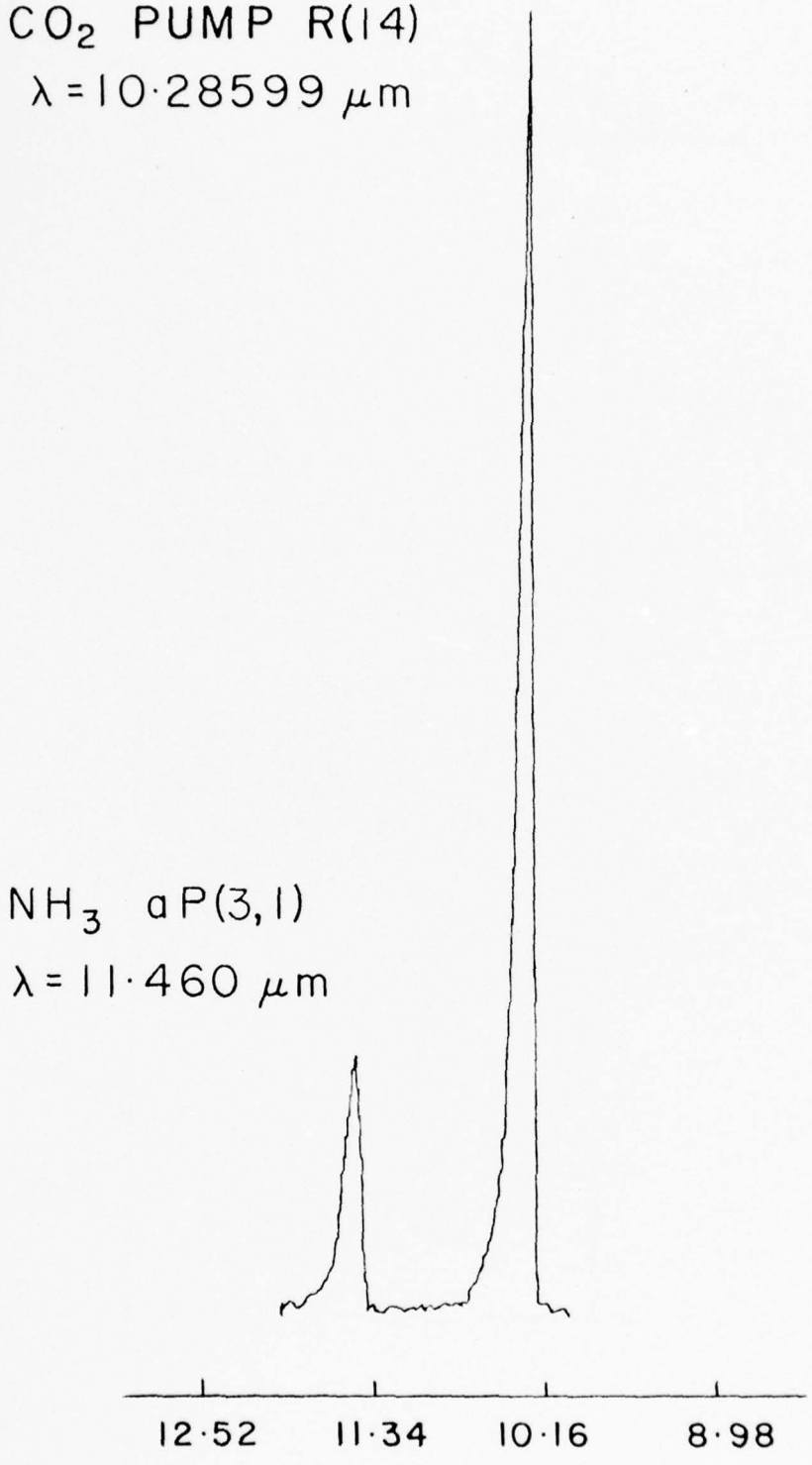

Figure 12. Wavelength scan showing 11.46 μm and 10.28 μm lines.

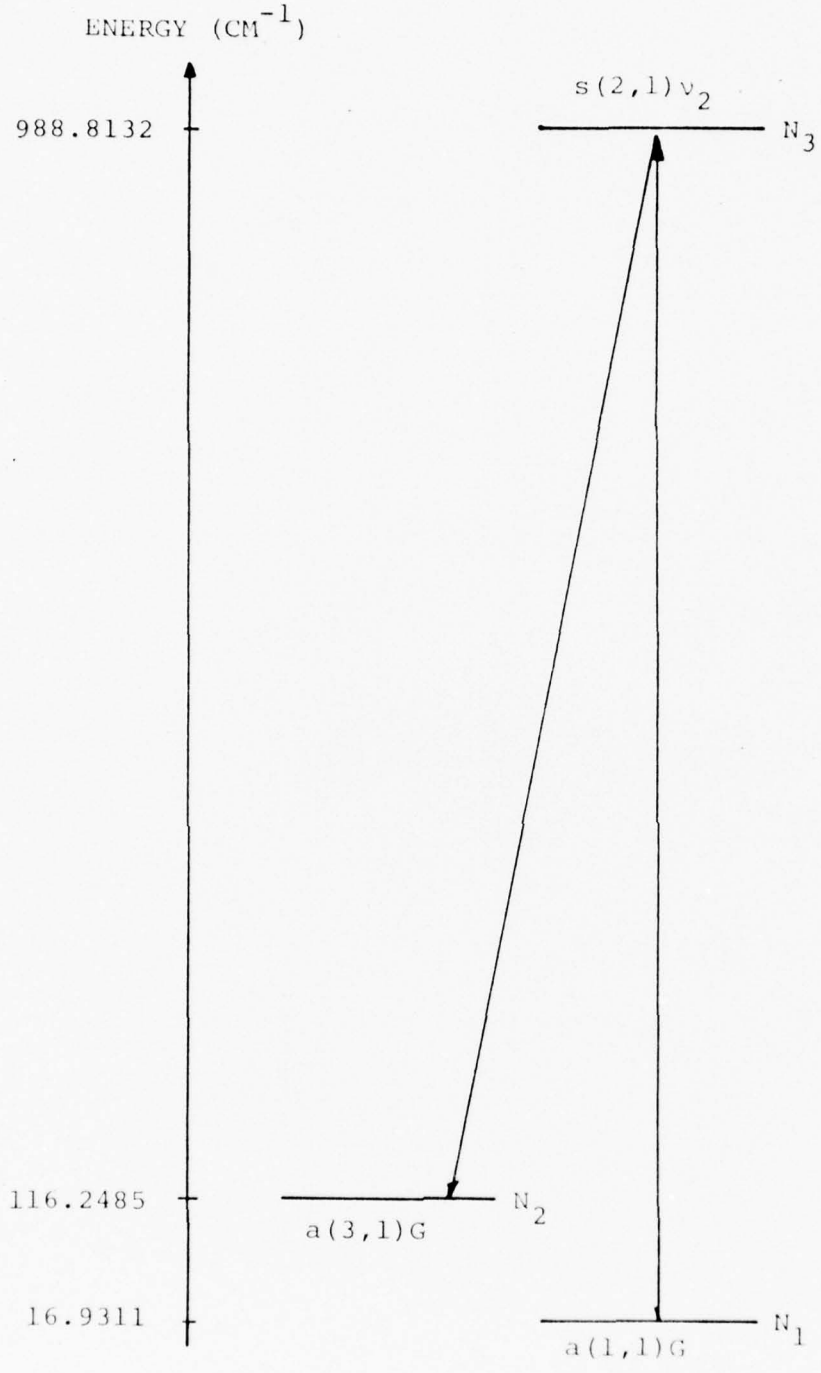

Figure 13. Simplified energy level diagram for the 11.46 μm transition.

$$S(I,K) = 2(4I^2 + 4I) \equiv \text{Nuclear Statistics} \qquad (2)$$

$$I = \frac{1}{2} \text{ for } NH_3$$

B,C usual spectroscopic meaning

$B = 9.944\ cm^{-1}$

$C = 6.196\ cm^{-1}$

E_{JK} = energy of the level

kT = Boltzmann factor times temperature ($\simeq 207\ cm^{-1}$ at room temperature)

(2J+1) = degeneracy factor

The actual population in a given level may be calculated by multiplying the total number of molecules present by the partition function. For the discussion here, only relative populations need be considered.

The diagram shown in Figure 13 will aid in the discussion. The population inversions, $N_3 - \frac{g_3}{g_2} N_2$ and $N_1 - \frac{g_1}{g_2} N_2$, are to be considered. For normal laser gain, the $N_3 - \frac{g_3}{g_2} N_2$ factor must be greater than zero. The most population that can be deposited into the ν_2 s(2,1) level occurs when the 10.286 μm transition is saturated. The population then becomes $\left(N_1 + \frac{g_1}{g_3} N_3\right)/2$ in both the Ga(1,1) and ν_2 s(2,1) states. The values for the relative population have already been determined

for these levels (see Table 3). The value of $\left(N_1 + \frac{g_1}{g_3} N_3\right)/2$ is determined to be 1.75×10^{-2}, this value is smaller than the population in N_2 which is 4.98×10^{-2}, hence a population inversion is impossible (under equilibrium considerations).

Table 3. Partition Function Calculation Results.

LEVEL	ENERGY	DEGENERACY	RELATIVE POPULATION
Ga(1,1)	16.9311 cm^{-1}	3	3.45×10^{-2}
Ga(3,1)	116.2485 cm^{-1}	7	4.98×10^{-2}
ν_2s(2,1)	988.8132 cm^{-1}	5	5.25×10^{-4}

For Raman-like gain the population inversion is determined by $N_1 - \frac{g_1}{g_2} N_2$. It is readily seen that an equilibrium population inversion can exist in this case.

The lack of a normal laser population inversion has led to the consideration that the observed line may be a stimulated Raman scattered (SRS) emission line. The SRS line would be expected to an off-resonant emission line as predicted by the three-level analysis of Javan[13] and others.[14,15]

A peculiar operating characteristic was noted during experimental studies of the 11.46 μm emission line. The output signal was strongly dependent on the input longitudinal mode structure. When the CO_2 laser mode locks, the energy of the

Table 4. Summary of 11.46 μm Data.

SPECTROSCOPIC SUMMARY

EMISSION FREQUENCY AND WAVELENGTH	872.565 cm^{-1}	11.460 μm
EMITTING TRANSITION	aP(3,1)	
ABSORBING TRANSITION AND FREQUENCY	aR(1,1)	971.881 cm^{-1}
CO_2 PUMP TRANSITION AND FREQUENCY	R(14)	971.930 cm^{-1}
PUMP MISMATCH	-1.445 GHz	-.049 cm^{-1}

TYPICAL OPERATING CHARACTERISTICS

CO_2 TEA LASER

MIXTURE	10:1:50	CO_2:N_2:He
POWER	1.0 MW	
PULSE LENGTH	160 nsec FWHM	
MODE CHARACTER		
LONGITUDINAL	SINGLE MODE	
TRANSVERSE	LOWER ORDER	

NH_3 11.460 μm EMISSION

CAVITY CONFIGURATION

CAVITY LENGTH	1.3m
OPTIMUM PRESSURE	∿1.2 TORR
OUTPUT POWER	UNKNOWN
CONVERSION EFFICIENCY	UNKNOWN

OFF-RESONANCE DATA RESULTS

$\Delta\nu_H$	23 MHz/TORR	26.273 MHz/TORR
11.46 μm DETUNING	1.139	1.217
10.288 μm DETUNING	1.352	1.445

pulse is spread out over a wide frequency spectrum around the center frequency. The output signal at 11.46 μm is random and very weak when mode locking occurs. Operating the CO_2 laser on a single longitudinal mode yields a stable signal with a relative output more than 20 times stronger than the mode locked case. The emission linewidth of the CO_2 laser strongly depends on the longitudinal mode structure of the pulse. This phenomenon is not observed for the 12.812 or 12.08 μm emission lines.

The lack of a population inversion and this peculiar operating characteristic has prompted investigation of the off-resonance behavior of the 11.46 μm emission line. This treatment follows a list of operating characteristics for the 11.46 μm emission line, given in Table 4.

2.37 Off-Resonance Behavior Study Process

The study of signal detuning is a subject of pressure-broadened spectroscopy. The method employed is described below, and consists of 6 steps.

1. Calculate emission matrix elements from available data, and obtain a pressure broadening rate for the transition of interest.

2. Calculate the appropriate Einstein A coefficient.

3. Calculate line center absorption to determine approximate length of experimental absorption cell.

4. Experimentally measure %T versus pressure squared.

5. Least squares fit data to the equation

$$\%T = a \exp(+b \ell p^2) \tag{3}$$

$a \simeq 1$ for good data

$b \equiv$ absorption constant

$p =$ pressure

$\ell \equiv$ length of the absorption cell.

6. The detuning is then calculated using

$$(\nu-\nu_o)^2 = \frac{-\lambda^2 A_{21} \Delta\nu_H \frac{g_2}{g_1}}{8\pi^2 b} \text{ (Hz)} \tag{4}$$

The calculations are presented next. One discrepancy is noted, the partitioning fractions calculated previously do not agree with the values used in this calculation. This however is a small difference and of little concern to the validity of these calculations.

The constants used are based on the data contained in the Curtis reference.[18] Additional references are contained in the bibliography of this reference.

The matrix element used is the matrix element for emission (not absorption) hence the initial state quantum numbers are used to determine the direction-cosine part of the matrix element. For absorption of the R(14) CO_2 laser transition, the absorbing transition is the aR(1,1). Reassigning this as an emitting transition would yield a $sP(2,1)^e$ identification.

Therefore

$$|\mu_{sP(2,1)e}|^2 = \mu^2 \frac{J^2-K^2}{J(2J+1)} = \frac{(.23)^2(2^2-1^2)}{2(2.2+1)}$$
$$= 1.587 \times 10^{-2} \text{ D} \tag{5}$$

The A coefficient is defined by

$$A = \frac{k^3\mu^2}{3\pi\varepsilon_o\hbar} = \left(\frac{\pi}{\lambda}\right)\frac{\mu^2}{3\pi\varepsilon_o\hbar} = \frac{\mu^2(D)}{\lambda^3(\mu m)} 2.9 \times 10^5 \text{ sec}^{-1} \tag{6}$$

Substitution of (4) into (5) with λ = 10.288 μm yields

$$A_{aR(1,1)} = 4.2265 \text{ sec}^{-1}$$

The next thing to be calculated is the line center absorption coefficient for the transition. The small signal absorption coefficient is needed so $I/I_{SAT} \simeq 0$ is assumed and Equation (7) results

$$\alpha = \frac{\lambda^2 A}{4\pi^2 \Delta\nu_H} - \left(\frac{g_2}{g_1}\right) N_1 + N_2 \quad N^{TOT} \tag{7}$$

$\Delta\nu_H$ is the linewidth parameter. N_1 and N_2 are partitioning fractions. $g_1(=2J_1+1)$ and $g_2(=2J_2+1)$ are the degeneracy factors of the lower and upper levels respectively. N^{TOT} is the total number of molecules per cubic centimeter and is a linear function of gas pressure. The standard value obtained from the ideal gas law is $3.3 \times 10^{16} \frac{\text{molecules}}{\text{cm}^3 \text{ torr}} = \frac{N^{TOT}}{p(\text{torr})}$.

A value of 23 ±3 MHz/torr was found in the literature[16] for $\Delta\nu_H$. N_1 was calculated to be .02001 for the Gs(1,1) level. The value for N_2 was 2 orders of magnitude smaller and is therefore neglected. The partitioning fraction does not include the inversion splitting effect. The partitioning of a given rotation state into its symmetric and antisymmetric levels must be related by a Boltzmann factor as shown below.

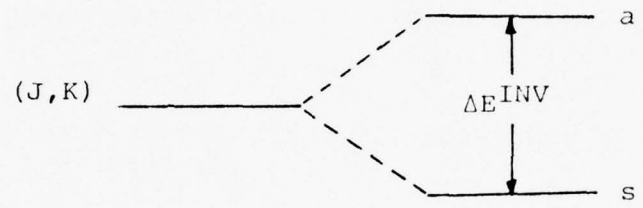

$$\frac{N_{JK_a}}{N_{JK_s}} = \exp(-\Delta E^{inv}/kT). \tag{9}$$

For the ground state where $\Delta E^{inv} \simeq 0.8\ cm^{-1}$ and room temperature (i.e., $kT \simeq 207\ cm^{-1}$) $N_{JK_a} \simeq N_{JK_s}$, so the population splits evenly between the two levels. An additional factor of 1/2 is required to account for this. This same approximation is less satisfactory for the ν_2 state $\left(\frac{N_a}{N_s} \simeq .84\right)$ and invalid the $2\nu_2$ state $\left(\frac{N_a}{N_s} \simeq 0.25\right)$. Rewriting Equation (7) with the assumptions just described yields

$$|\alpha| = \left|\frac{\lambda^2 A}{4\pi^2 \Delta\nu_H}\left(\frac{g_2}{g_1}\right) N_1 N^{TOT}\left(\frac{1}{2}\right)\right| \tag{10}$$

Substitution of all the values appropriate for the aR(1,1) absorption transition yields

$$\alpha(1 \text{ torr}) = 2.691 \text{ cm}^{-1}$$

Similarly for the aP(3,1) with a transition wavelength of 11.46 μm yields and emission transition moment of 2.821 $\times 10^{-2}$ D and an A coefficient of 5.436 sec^{-1}. The population partitioning fraction is found to be 0.02873. Using all these values leads to a line center absorption coefficient of 2.662 cm^{-1}. These results are tabulated below.

Table 5. Calculated Parameters for Off-Resonance Study of 10.288 and 11.46 μm.

CONSTANT	10.288 μm	11.460 μm
ABSORBING TRANSITION	aR(1,1)	aP(3,1)
$\lvert\mu^e\rvert^2$ (D)	1.587×10^{-2}	2.821×10^{-2}
A(sec^{-1})	4.2265	5.436
N_1	0.02001	0.02873
(1 torr)(cm^{-1})	2.691	2.662
$\Delta\nu_H \frac{\text{MHz}}{\text{TORR}}$	23	23

2.38 Experimental Determination of Off-Resonance Behavior

It can be shown that for off-resonance pumping the small signal absorption coefficient (Equation (11)) is proportional to the square of the pressure of the absorber. This dependence

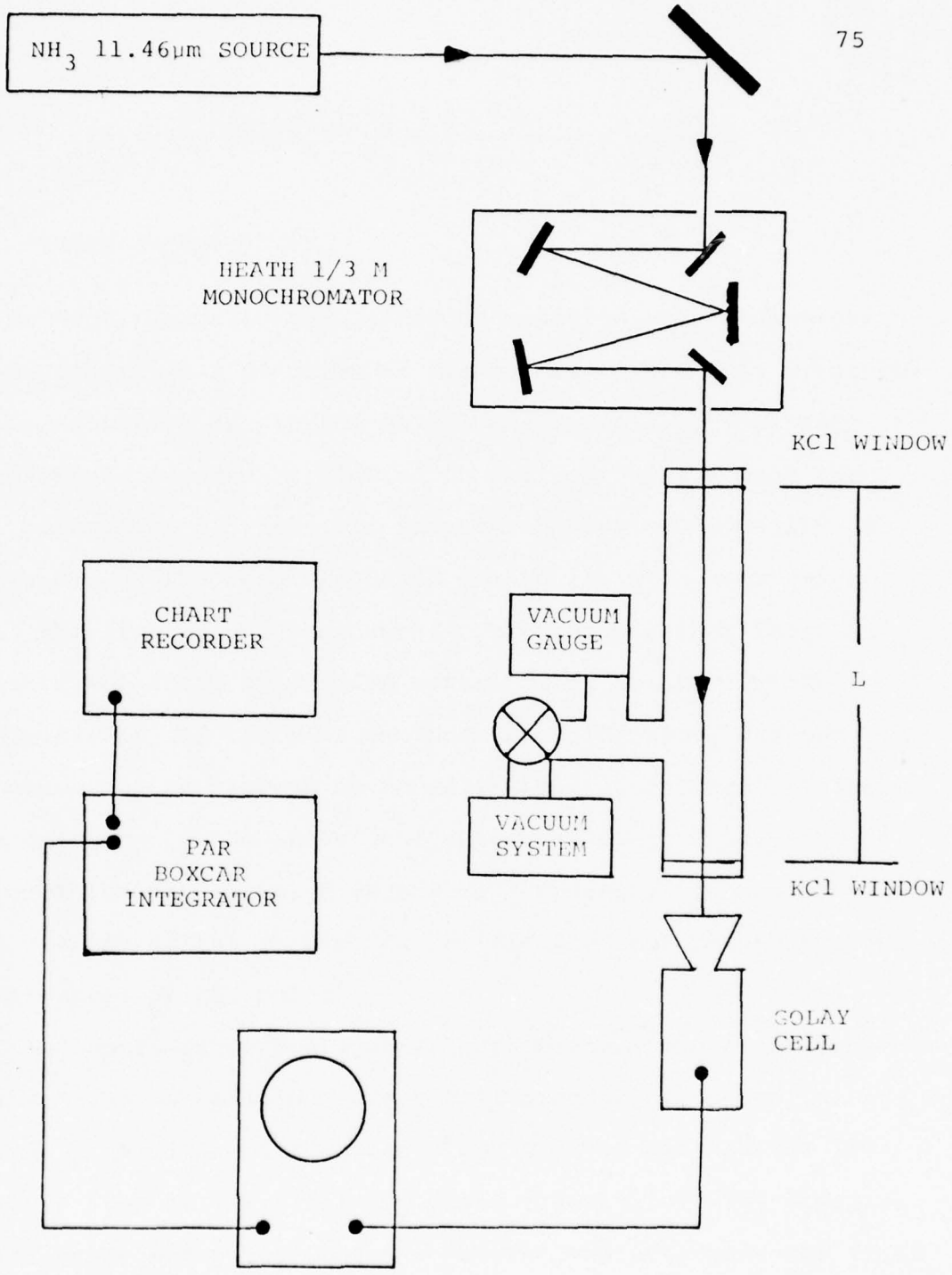

Figure 14. Experimental configuration for measuring off-resonance behavior of the 11.46 μm emission line.

$$\alpha(\nu) = \frac{\lambda^2 A_{21}}{8\pi^2}\left(N_2 - \frac{g_2}{g_1} N_1\right)\frac{\Delta\nu_H}{(\nu-\nu_o)^2} = \frac{mp^2}{(\nu-\nu_o)^2} \qquad (11)$$

assume $(\nu-\nu_o) >> \delta\nu_D$

may be experimentally determined by measuring the transmission of the signal as a function of the square of the cell pressure. The transmission is plotted on a logarithmic axis, whereas the pressure squared is plotted on a linear axis. Once the data points are plotted, off-resonance behavior is easily determined. If the resulting data points lie along a straight line, the line is off-resonance. This assumes that there is no other absorbing transition contributing to the overall transmission. If there is another absorbing line, its contribution may be removed by recalling that the overall absorption is a sum of the individual absorbing components. The slope of the transmission versus cell pressure squared plot is a measure of the absorption coefficient dependence on pressure squared of the cell.

An experimental configuration to measure the transmission of the 11.46 μm emission versus cell pressure is shown in Figure 14. A similar configuration was used to measure the frequency offset of the R(14) CO_2 laser transition. The spectrometer, which serves to frequency select and attenuate the 11.46 μm emission line, was replaced by an absorbing gas cell. The CO_2 measurement was accomplished with a frequency stabilized

CW laser mounted in an invar structure.

The results of the two experiments are shown in Figures 15 and 16. Note the small amount of scatter that is observed in Figure 15, this is a direct result of doing the measurement in a CW (continuous wave) rather than pulsed mode. To obtain some of the higher pressure points a shorter cell was needed to increase the detection signal-to-noise ratio. The correction factor is easily attained by raising the transmission measured to the ratio of the new length to the old length power. This is needed so that all data points can be plotted on the same graph and is expressed mathematically by

$$I_1(\ell_2) = I_2\left(\frac{\ell_2}{\ell_1}\right) = I_o \exp(-\alpha \ell_1/\ell_1\ell_2) \qquad (12)$$

$\ell_1 \equiv$ old length

$\ell_2 \equiv$ new length

$I_o \equiv$ initial intensity

$I_1 \equiv$ transmitted intensity through ℓ_1

$I_2 \equiv$ transmitted intensity through ℓ_2.

A least squares fit to the function $y = a\ell^{bx}$ (y is transimission, x is pressure squared) was then accomplished for the two cases. The results of these calculations are tabulated below.

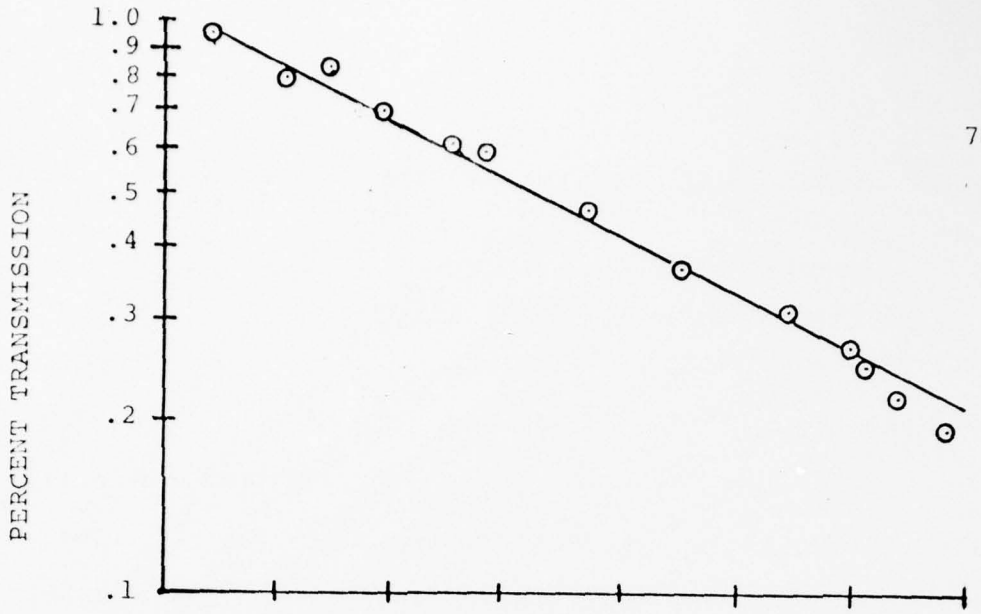

Figure 15. CW CO_2 (R(14) (10.288 μm) absorption in NH_3

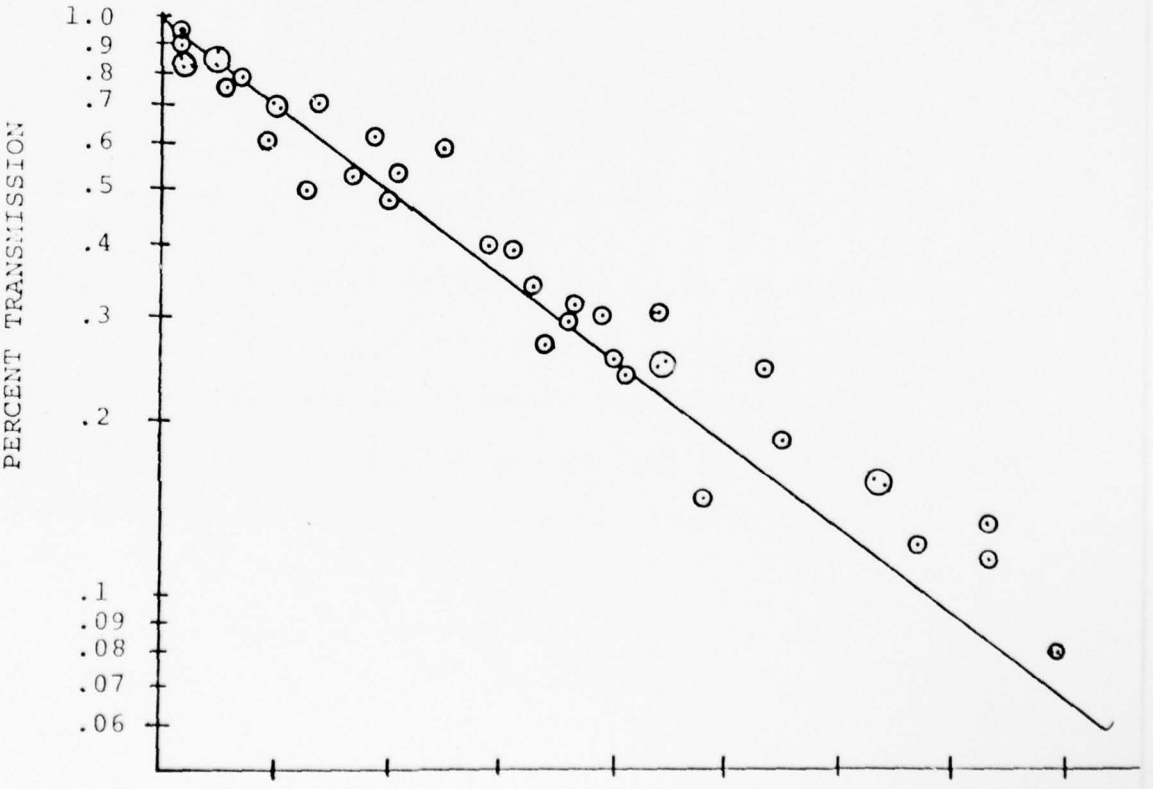

Figure 16. NH_3 self-absorption at 11.46 μm.

Table 6. Experimental Data Summary for Off-Resonance Study of 10.28 and 11.46 μm Lines.

	R(14) 10.288 μm	11.46 μm
TRANSITION	aR(1,1)	aP(3,1)
FREQUENCY	971.8821	872.5647
NEAREST ABSORPTIONS		
LOWER	aQ(1,1)967.8854	aP(3,2)871.7371
HIGHER	2sR(1,0)987.7743	872.9884
CELL LENGTH = ℓ	24.85 cm	24.85 cm
NUMBER OF DATA POINTS	13	41
a	1.1077	1.0017
b	-4.8738×10^{-3}	-6.7402×10^{-3}
$\frac{\alpha}{p^2} = b/\ell$	-1.9613×10^{-4}	-2.7124

The actual frequency detuning may be calculated using Equation (11). The population in level N_2 is small compared to the ground state and is therefore neglected. The additional factor of $\frac{1}{2}$ is included to account for the inversion splitting of the ground state. The resulting equation is (12)

$$(\nu-\nu_o)^2 = \frac{-\lambda^2 A_{21} \Delta\nu_H \frac{g_2}{g_1}}{16\pi^2 \alpha_{measured}} = 1.8271 \times 10^{18} \text{ sec}^{-2} \quad (12)$$

$$\Delta\nu = (\nu-\nu_o) = 1.3517 \times 10^9 \text{ Hz} = 1.3517 \text{ GHz}$$

The value measured experimentally by Oka[12] is 1.445 GHz. This value was used to recalculate the pressure broadening coefficient. The new value for $\Delta\nu_H$ is 26.273 MHz/torr. Performing a similar calculation for the 11.46 μm transition with $\Delta\nu_H$ = 23 MHz/torr yields a detuning of 1.139 GHz. With $\Delta\nu_H$ = 26.273 MHz/torr the calculation yields a detuning of 1.217 GHz.

The experimental frequency detuning results for the 11.46 μm emission and the 10.288 μm absorption are 1.139 GHz and 1.3517 GHz for a pressure broadening coefficient of 23 MHz/torr and 1.217 GHz and 1.445 GHz for $\Delta\nu_H$ = 26.273 MHz/torr.

2.38.1 Discussion of Detuning Results

Excellent agreement between Oka's observed detuning and our measurement of the CO_2 R(14) emission line with the sR(1,1) transition in NH_3 was obtained. The use of the frequency stabilized CW CO_2 laser made the data acquisition for the experiment relatively easy. The same can not be said for the 11.46 μm emission line. The data was difficult to obtain and once analyzed appears to be in error.

The frequency offset of the emission line at 11.46 μm appears to be shifted closer to resonance than the pumping transition. This is not the expected case. A single photon

exhibits a field which Stark shifts the appropriate levels out of resonance, the observed case is the opposite. Immediate explanations of this observation are not available. Experimental errors could occur from a number of different sources. An additional absorption line may be contributing to the measured transmittance. This is very doubtful because of the high resolution spectra observed by Curtis,[28] shows relative isolation.

It is known that the pressure broadening coefficient of NH_3 is dependent on its J and K quantum numbers.[17] The actual dependence is not perfectly clear. This is probably the biggest single reason for the discrepancy. Measurement of the emission linewidth as a function of pressure should determine if this is the cause.

The discrepancy in the frequency offsets may involve some non-linear process. An expression for the signal gain of the three-level system shown in Figure 17 has been derived by Coleman.[15] Similar results have been obtained by Yajima[14] and Javan.[13] Figure 18 depicts several signal gain curves as a function of pump detuning in terms of linewidths. Constant pump intensity is assumed. For near resonant conditions, a double peak appears in the gain curve. For a cavity configuration, the gain is multiplied by the Q of the cavity. Therefore, it seems plausible that both components might be observed in the emission near the signal frequency for different

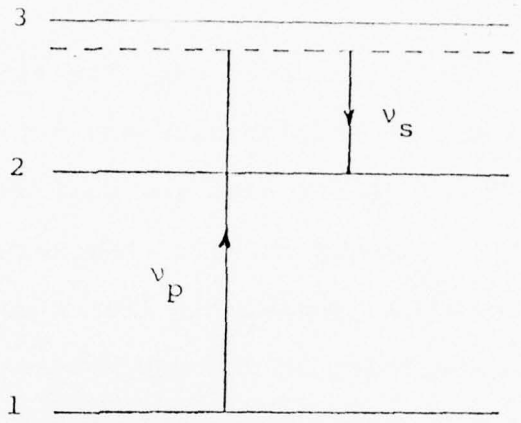

Figure 17. Three-level system (μ_{13}, $\mu_{32} \neq 0$, $\mu_{12} = 0$).

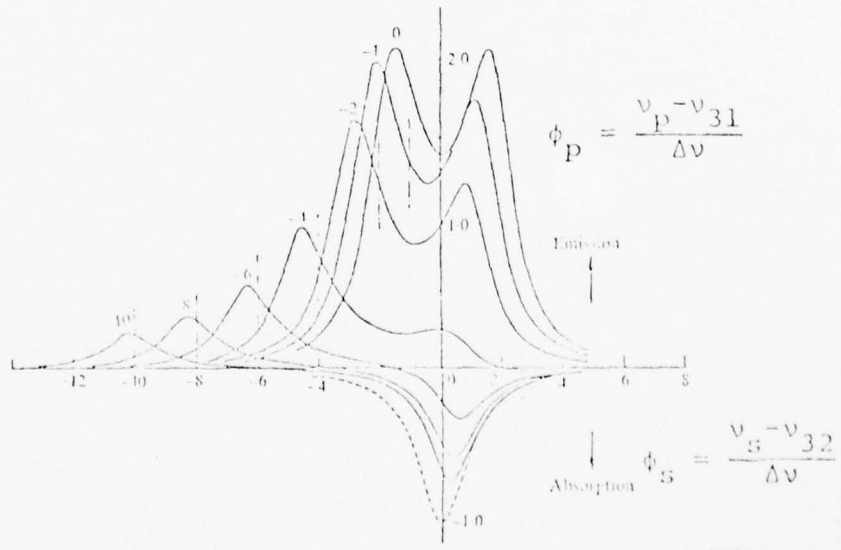

Figure 18. Theoretical shapes of the signal line under resonant and off-resonant pumping with $w_p = 3$ in a three-level system, where $\nu_{31}/\nu_{32} = 9.47$ and $\phi_p = \nu_p - \nu_{31}/\Delta\nu$.[14]

component gains. If this were the case, a suitable explanation could be obtained. During the transmission versus cell pressure experiments, instability was observed at low pressures (< 1 torr) for the transmitted 11.46 μm signal. Addition of more NH_3 to the absorption cell eliminated the majority of the instability. This may or may not be experimental evidence for the existence of a two component emission line.

Whatever the case, this problem should receive additional attention. As suggested earlier, an infrared-microwave double resonance experiment may indeed resolve these questions.

The results indicate that the 11.46 μm emission line is off-resonance. Further conclusive statements regarding its Raman nature require further investigation.

2.39 High Pressure Pure Rotation Transitions in NH_3

Superfluorescent FIR emission at 26.44 μm has been observed by optically pumping the sR(4,3) $\nu_2 \rightarrow 2\nu_2$ "Hot Band" transition of NH_3. The pump source is a single-mode 1 MW CO_2 TEA laser, operating on the P(24) (9.586 μm)transition. Two additional FIR emission lines were observed by optically pumping a cavity. The experimental results have been spectroscopically identified and are summarized in Figure 19.

The three emission lines all exhibit the same pressure dependence. All the lines emit at pressures exceeding 10 torr. This feature is unusual for pure rotation transitions. Rotational relaxation usually overcomes the population inversions needed for gain at pressures greater than 5 torr. Higher pressures are obtainable by using much higher pump powers. The lines observed do not require the higher pumping power.

The experimental apparatus used for the experiment has been described earlier. One modification has been implemented which increases the FIR output power by a factor of two. A 5.6 mm bore Pyrex capillary tube, with hole-coupled mirrors for feedback, is used as the optically pumped laser cavity. This modification serves to confine the pumping radiation to the active region of the pumped cavity. Superfluorescent emission was observed by removing one or both of the feedback mirrors. An approximate factor of two decrease in the output power is observed when no feedback is used as compared to a single feedback mirror.

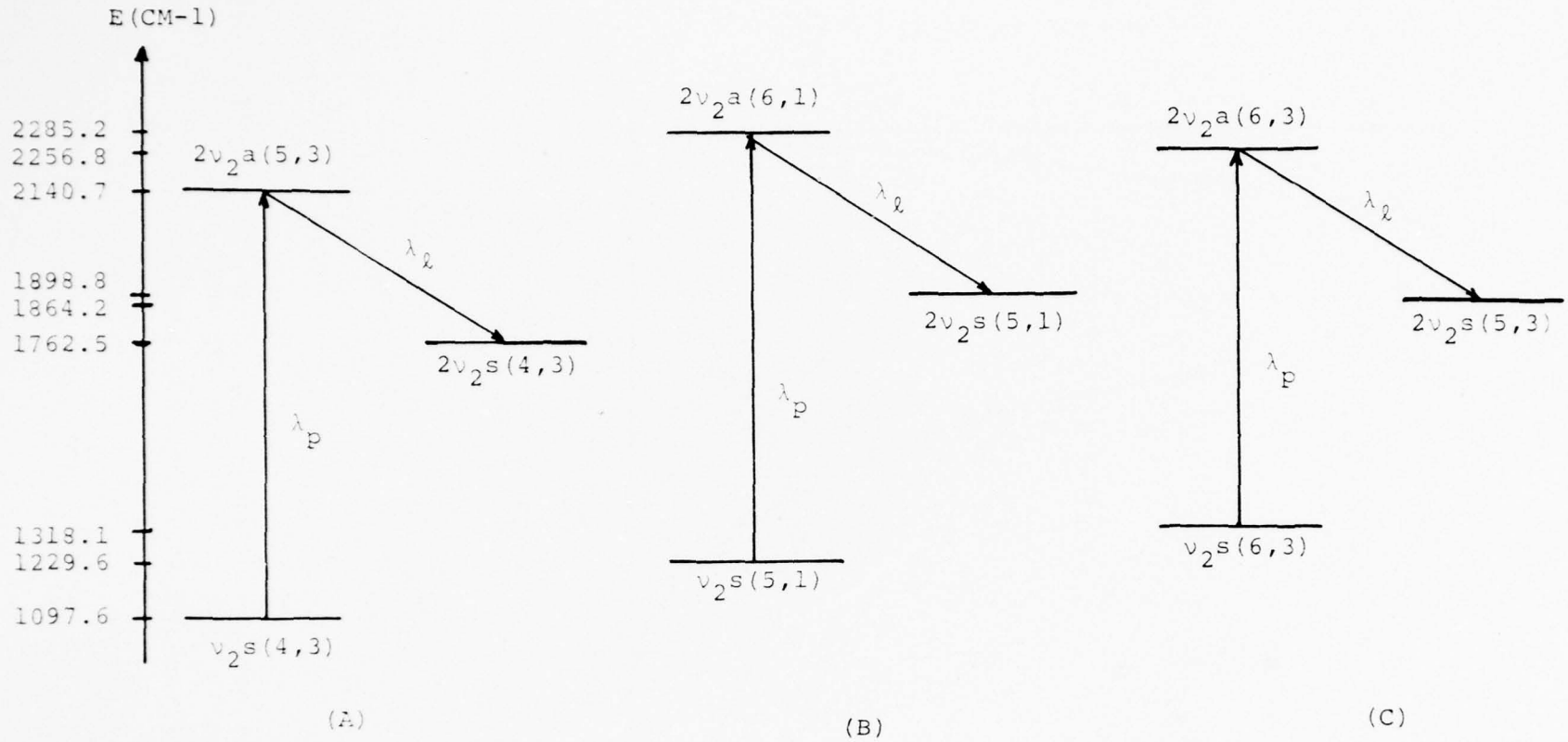

FIG.	λ_e(μm)	λ_p(μm)	CO_2 LINE	ABS. LINE	$\nu_{ABS}-\nu_2$(cm-1)	COMMENT
A	26.44	9.586	P(24)	sR(4,3)	.01	SUPERFLUORESCENT
B	25.88	9.473	P(10)	sR(5,1)	.07	
C	25.47	10.653	P(26)	sQ(6,3)	.04	

Figure 19. Summary of newly found NH_3 emission lines.

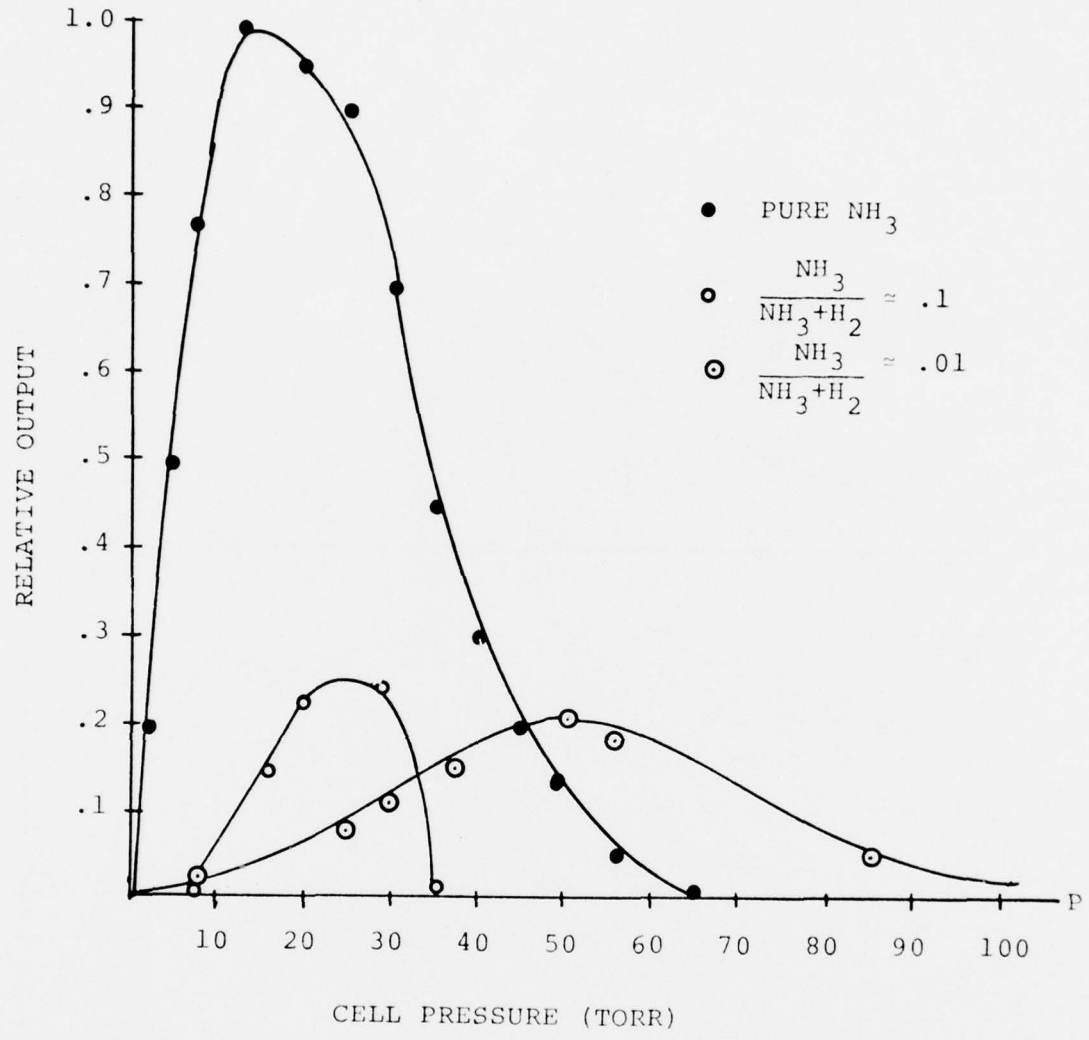

Figure 20. Relative output vs. cell pressure for 26.3 μm emission line for various mixtures of hydrogen and NH_3. Power input constant (∿ 1 MW) cavity configuration.

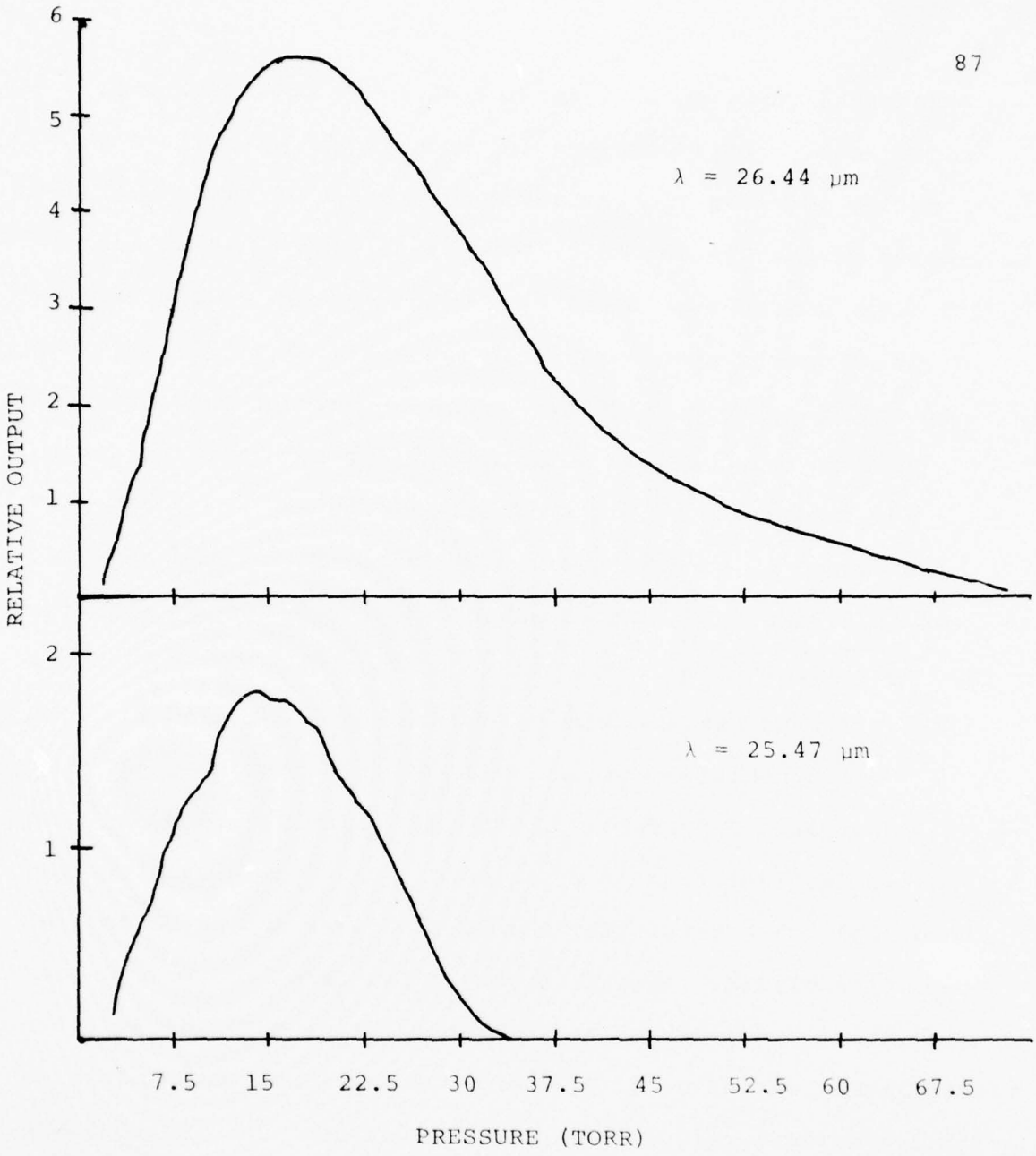

Figure 21. Relative output power versus pressure for 26.44 μm and 25.47 μm emission lines.

The operating pressure for the 26.2 μm superfluorescent emission line is higher than for the same line in a cavity. Figure 20 shows relative output versus cell pressure curves for the 26.44 μm line in an unmodified cavity. Various concentrations of hydrogen have been added as a buffer gas. For a mixture 100:1 (H_2:NH_3) operating pressures in excess of 100 torr were obtained. Subsequent studies using different concentrations have yielded emission at pressures greater than 200 torr. Figure 21 depicts a pressure curve of the 26.44 μm line in the modified cavity. Figure 21 shows a relative output versus cell pressure curve for the 25.47 μm line. The two curves are normalized to the same relative output, but note that the relative output scales are different.

The high operating pressure may be explained quite simply. Most optically pumped pure rotation transitions pump molecules from the ground state to a vibrational state determined by the frequency of the pump laser. For "hot band" absorptions the level being pumped is some vibrationally excited state. The equilibrium population distributions (i.e., partition functions) are considerably lower in the vibrationally excited state as compared to the ground state. The actual difference is determined by a Boltzmann factor and any degeneracy terms that are appropriate. In NH_3 the lower state being pumped is approximately 1000 cm^{-1}. This leads to a factor of e^{-5} difference in populations. Therefore additional pressure

is needed to obtain workable population in the vibrationally excited ν_2 state.

Another factor contributing to the high operating pressures is the existence of large inversion splittings in the $2\nu_2$ state of NH_3 ($\sim$ 285 cm^{-1}). Rotational relaxation in the $2\nu_2$ state is not a resonant process and hence much translational energy is required to conserve energy in the relaxation process. This implies that the $2\nu_2$ excited state lifetimes are longer in the $2\nu_2$ than in the ground or ν_2 states.

Gulberg et al.[5] reported emission at 154.53 μm and 276.53 μm by pumping the same sR(4,3) $\nu_2 \rightarrow 2\nu_2$ "hot band" absorption. The pressures used in his experiment are similar to what we have observed.

In summary, we report superfluorescent emission at 26.44 μm and emission at 25.88 μm and 25.47 μm optically pumped by CO_2. The experimental results are summarized in Figure 19.

2.40 Optical Pumping of PH_3

The major part of this year's experimental investigation has dealt with V-R transitions in optically pumped NH_3. NH_3 is an example of a pyrimidal symmetric top molecule. PH_3 is a similar molecule with negligible inversion splittings. The optical properties of PH_3 are expected to be very similar to NH_3. The similarities between PH_3 and NH_3 has prompted the study of an optically pumped tunable laser in PH_3. The results to be presented are the results of a literature search and

experience gained from the study of NH_3. Experimental confirmation of this idea has not yet been accomplished although discrete laser signals have been observed.

Shimizu[19] recently investigated the laser Stark spectroscopy of PH_3 using N_2O and CO_2 lasers. The data obtained in this referrence identify the laser pump lines and the corresponding absorbing transitions.

Yin and Rao[20] have experimentally measured and identified many of the transitions in the 8-12 μm region of PH_3. Molecular constants to determine the energy levels are also presented. A computer program was written (with the aif of J. Niesen) to calculate the energy levels and possible transition frequencies using this data.

Unlike NH_3, both the ν_2 and ν_4 modes are accessible using a CO_2 pump laser. The analogous case to NH_3 is depicted in Figure 22. The ν_2 band is pumped with Frequency I, and emission can occur on frequencies II, III or IV. Cascade emission (IV) is also shown and may occur. Of the cases listed in the figure, the ones with the smallest pump detunings ($\Delta\nu$) are the most likely candidates.

The feature that makes PH_3 a likely candidate for an optically pumped tunable laser source is the accessibility of the ν_4 band. The ν_2 and ν_4 bands of a pyrimidal symmetric top molecule are Coriolis coupled.[21] This means that there exists a matrix element between the ν_2 and ν_4 states. Transitions of

CO_2 9μm	(J,K)	I	II CM^{-1} μm	III CM^{-1} μm	IV CM^{-1} μm	V CM^{-1} μm	Δ(GHz)
P(26)	(5,4)	1041.387	925.856	51.315	53.34	62.191	-3.6
			10.800	194.875	187.473	160.795	
P(24)	(5,5)	1043.143	927.570	51.192	53.44	62.133	.5
			10.781	195.343	187.715	160.945	
R(10)	(9,7)	1071.904	881.758	85.544	88.696	101.450	-.3
			11.341	116.399	112.745	98.571	
R(14)	(9,8)	1074.629	868.555	85.479	88.725	117.349	.6
			11.513	116.988	112.708	85.216	
R(10)	(10,4)	1071.904	888.383	94.268	97.321	86.200	-.8
			11.257	106.081	102.753	116.009	
R(18)	(10,7)	1077.358	873.750	94.135	94.840	108.768	-1.3
			11.445	106.230	105.441	91.939	

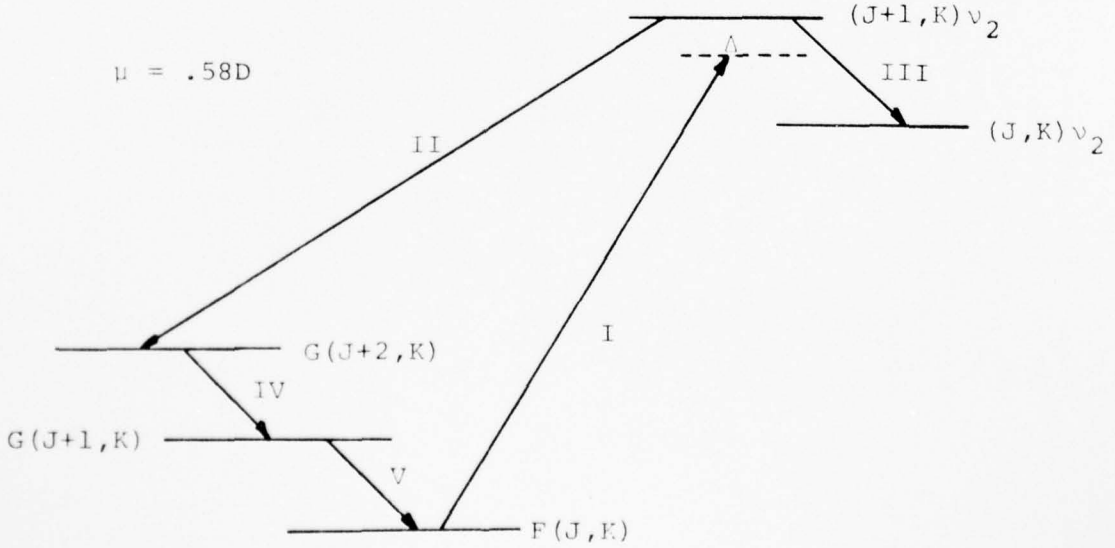

Figure 22. Optically pumped PH_3 possibilities. I. the ν_2 band.

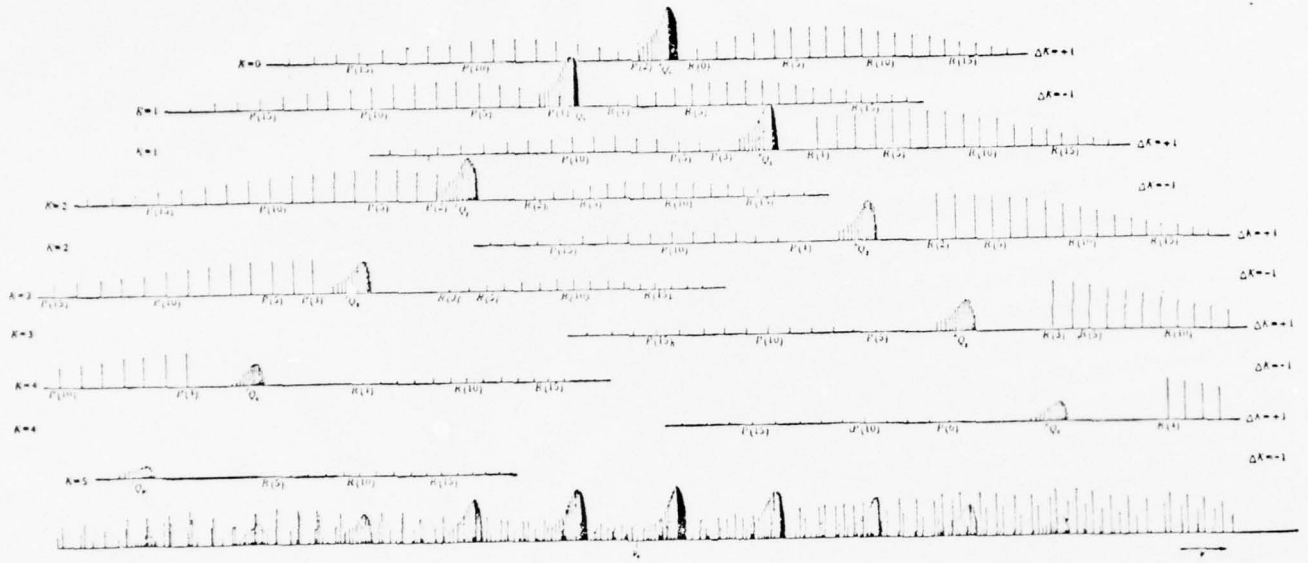

Figure 23. Sub-bands of a $\perp$ band and complete $\perp$ band of a symmetric top. The complete band is shown in the bottom strip. The spectrum is drawn under the assumption that A' = 5.18, A" = 5.25, B' = 0.85 cm^{-1} and $\zeta_i = 0$. The intensities were calculated for a temperature of 144°K. It should be realized that if the lines of an individual Q branch are not resolved the resulting "line" would stand out much more prominently than might appear from the spectrum given.[22]

AD-A038 518 ILLINOIS UNIV AT URBANA-CHAMPAIGN DEPT OF ELECTRICAL --ETC F/G 20/5
FREQUENCY TUNABLE LASER SOURCES.(U)
MAR 77 P D COLEMAN AF-AFOSR-2988

UNCLASSIFIED UILU-ENG-77-2548 AFOSR-TR-77-0379 NL

2 OF 2
ADA038518

END
DATE FILMED
5-77

this type have been observed in NH_3[18] and are expected in PH_3. The strength of the Coriolis coupling depends on the energy mismatch of the perturbed levels. In NH_3 the mismatch is the order of 600 cm^{-1}, while in PH_3 the mismatch is only 100 cm^{-1}. Therefore the perturbation (and hence the matrix elements) are expected to be larger for PH_3 than for NH_3.

The ν_4 mode is a perpendicular vibration (i.e., the dipole is vibrating perpendicular to the symmetric top axis.). The dipole selection rules for perpendicular type vibrations in a symmetric top molecule are

$$\Delta J = 0, \pm 1 \qquad \Delta K = \pm 1 \ .$$

To a good approximation, rotational relaxation obeys the dipole selection rules. The K part of the selection rule implies that the entire K manifold of a given J value should relax very quickly, since all levels in the manifold are nearly equal in energy. The rotational relaxation to other J states is expected to be somewhat slower, that is, similar to a parallel band relaxation. This will allow entire K manifold of a given J value to be pumped at moderate pressures. A schematic diagram, detailing the spectra of a typical perpendicular V-R band is shown in Figure 23. The density of lines shown should allow for emission on several of the closely spaced K subgroups yielding tunable radiation about the center frequencies. The possible emission center frequencies are

CO_2 PUMP TRANSITION 9 μm	ABSORBING TRANSITION	Δ(GHz)	II+ (CM^{-1}) II-	III+ (CM^{-1}) III-
P(26)	$^{P}P(7,7)$	-1.1	NA 47.3	69.7 60.4
P(20)	$^{P}P(8,3)$	-	66.2 61.2	68.0 64.9
P(18)	$^{R}P(10,2)$	.4	85.2 77.9	55.9 51.3
P(10)	$^{R}P(9,3)$	-	77.7 67.7	60.9 54.7
P(8)	$^{R}P(9,5)$	-1.5	80.3 65.3	57.8 48.5
P(6)	$^{P}P(7,1)$	.3	54.7 NA	73.6 NA

$\omega_1 \pm \nu_4(J,K) \rightarrow \nu_4(J-1,K\pm1)$

$\omega_2 \pm \nu_4(J,K) \rightarrow \nu_2(J+1,K\pm1)$

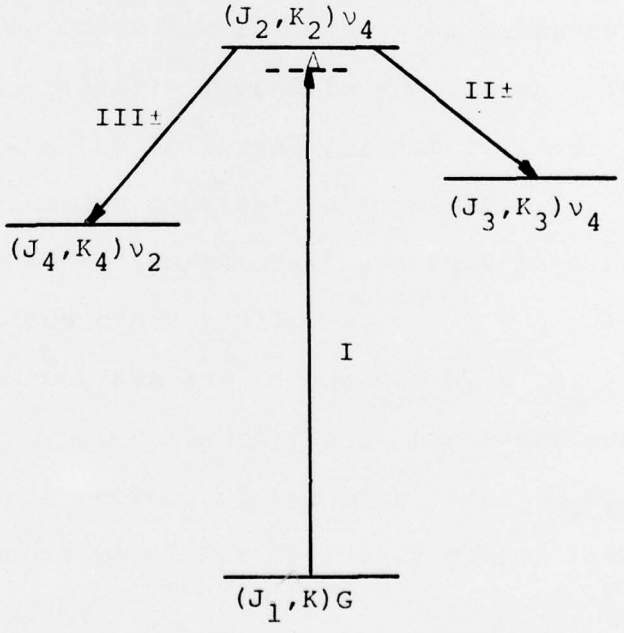

Figure 24. Optically pumped PH_3 possibilities. II. the ν_4 band.

listed in Figure 24. The transitions listed in Figure 24 include the ν_4 pure rotation ($II_{\pm}$) transitions and the $\nu_2 \rightarrow \nu_4$ V-R transitions ($III_{\pm}$). The listed V-R transitions are P type ($\Delta J = -1$) transitions, since these are most probable. Emission may occur on transitions similar to the ν_2 band, but have not been considered here.

A way of generating tunable FIR radiation by optical pumping of PH_3 has been presented. Possible emission wavelengths have been determined from the available spectroscopic data. The calculations are based on a literature search and the experience gained by studying NH_3. Experimental investigation is necessary to confirm these predictions.

2.41 Optically Pumped Spherical Top Molecules

Spherical top molecules fall into the category of a good candidate for an optically pumped tunable laser. That is, spherical tops have the following characteristics:

1. small rotation constants are possible.
2. No permanent dipole moment and thus pure rotation transitions are not allowed.
3. absorption bands are accessible by a CO_2 laser.

Spherical top molecules represent our least successful experimental investigations of the past year. O_sO_4, SiF_4, and CCl_4 were all investigated for optically pumped laser action with negative results.

The subsequent questions of why the pumping schemes did not work prompted further theoretical investigation. It was soon realized that spherical top molecules, with their high level of degeneracy, have non-typical equilibrium population distributions at room temperature. At room temperature only 30% of the molecules are in the vibrational ground state. This fact led to calculation of the vibrational partition function for the spherical top molecules studied. A partial energy level diagram for O_sO_4 is shown in Figure 25.

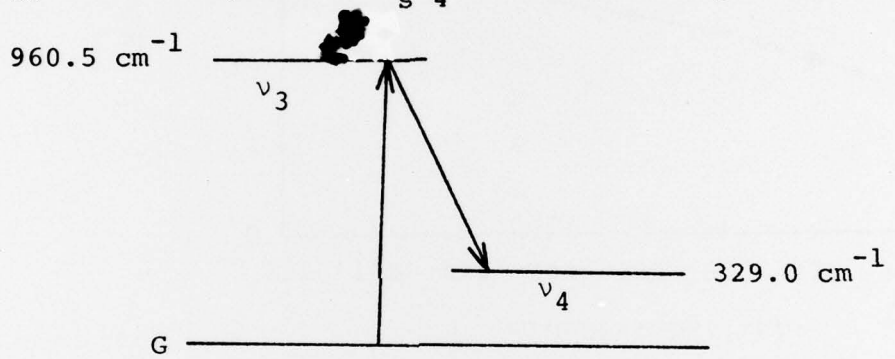

Figure 25. Partial energy level diagram of O_sO_4.

The calculation neglected the rotational part of the partition function, because it was hoped to invert the entire vibrational manifold. The partition function was calculated at various temperatures. Since a population inversion was desired between the ν_3 and the ν_4 vibrational levels the population distributions saturation of the absorbing transition from the ground to ν_3 state is assumed (i.e., $N_{G_{SAT}} = N_{\nu 3_{SAT}} = \frac{N_G + N_{\nu 3}}{2}$). The relative populations are plotted in Figure It is seen that a population inversion cannot be had at

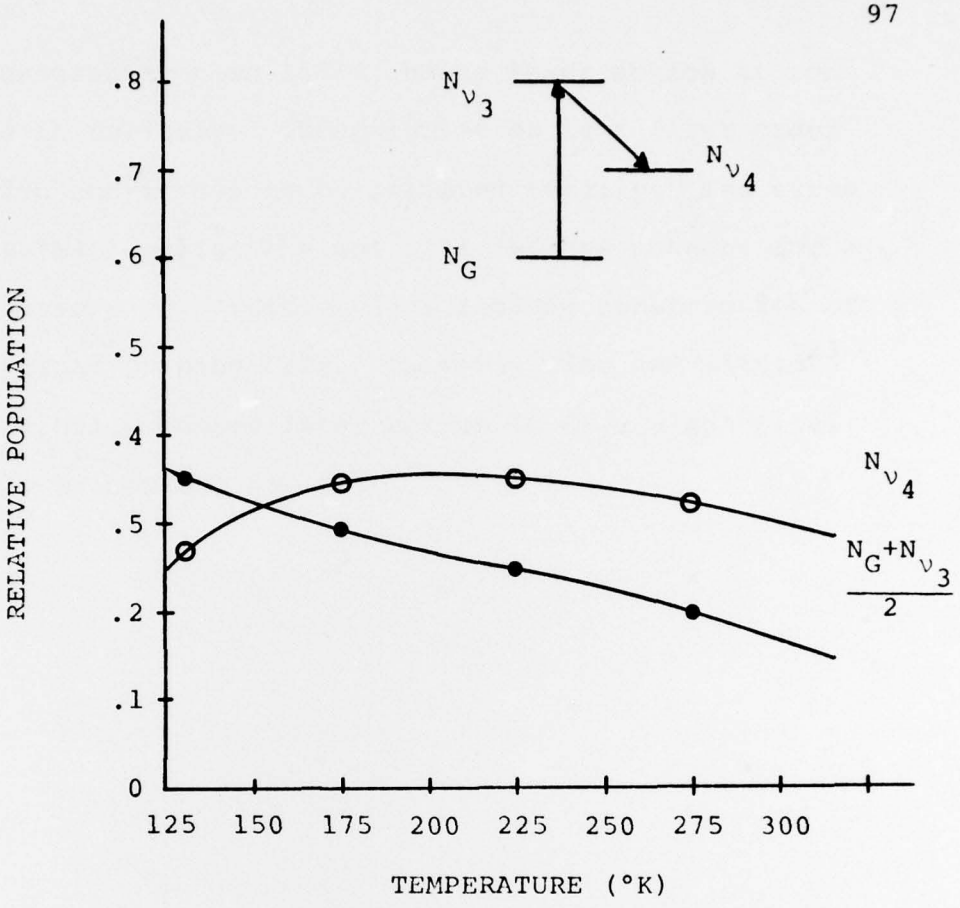

Figure 26. Relative population distribution of O_sO_4 as a function of temperature.

1) Saturation of transition from $G \rightarrow \nu_3$ is assumed

$$\left(\text{i.e., } N_G(SAT) = N_{\nu_3}(SAT) = \frac{N_G + N_{\nu 3}}{2}\right) .$$

2) Rotational part of partition function neglected

(i.e., $\Sigma f_{JK}(v) = 1$).

temperatures greater than 150°K, hence laser action at room temperature is unlikely. The calculation is a first order approximation and is not to be believed totally. The curve illustrates that cooling the gas will improve chances for a population inversion. Future plans include construction of a cooled optical pumping cell. Recently Tiee and Wittig[23] reported optically pumped laser action in CF_4, a spherical top molecule by cooling the gas.

LIST OF REFERENCES

1. M. Rosenbluh, R. J. Temkin and K. J. Button, "Submillimeter Laser Wavelength Tables, Applied Optics," 15, No. 11, 2635 (1976).

2. T. Y. Chang and O. R. Wood, "Optically Pumped 33-atm. CO_2 Laser", Appl. Phys. Lett., 23, No. 7, 370 (1973).

3. Proposal on Frequency Tunable Laser Sources, prepared by Electro-Physics Laboratory for Air Force Office of Scientific Resources, June 1974.

4. T. Y. Chang and J. D. McGee, "Laser Action at 12.812 μm in Optically Pumped NH_3", Appl. Phys. Lett., 28, No. 9, 526 (1976).

5. K. Gullberg, B. Hartmann and B. Kleman, "Submillimeter Emission from Optically Pumped $^{14}NH_3$", Physica Scripta., 8, 177 (1973).

6. Proceedings: Lasers for Isotope Separation Conference, April 13-14, 1976, Albuquerque, New Mexico.

7. E. J. Danielewicz, E. G. Malk and P. D. Coleman, "High Power Vibration-Rotation Emission from $^{14}NH_3$ Optically Pumped Off Resonance", Appl. Phys. Lett., 29, No. 9, 557 (1976.

8. S. M. Fry, "Optically Pumped Multiline NH_3 Laser", Opt. Commun., to be published.

9. K. J. Kim, unpublished data.

10. T. Y. Chang and J. D. McGee, "Off-Resonant Infrared Laser Action in NH_3 and C_2H_4 Without Population Inversion", Appl. Phys. Lett., 29, No. 11, 725 (1976).

11. T. A. DeTemple and A. V. Nurmikko, "Dynamics of Single Mode Operation of High Pressure CO_2 Lasers", Opt. Commun., 4, 231 (1971).

12. T. Oka, in Proceedings of the International Conference on Laser Spectroscopy, edited by R. G. Brewer and A. Mooradian, (Plenum, New York, 1974), p. 413.

13. A. Javan, "Theory of a Three-Level Maser", Phys. Rev., 107, 1579 (1957).

14. T. Yajima, "Three-Level Maser Action in a Gas, I", J. Phys. Soc. Japan, 16, 1594 (1961).

15. P. D. Coleman, "Proposal on Nonlinear Spectroscopy of Molecular Gases: Frequency Tunable and FIR Lasers", Prepared by Electro-Physics Laboratory for Air Force Office of Scientific Research, August 1976.

16. S. M. Freund and T. Oka, "Infrared-Microwave Two-Photon Spectroscopy: The ν_2 Band of NH_3", Phys. Rev. A, 13, No. 6, 2178 (1976).

17. J. S. Murphy and J. E. Boggs, "Collision Broadening of Rotational Absorption Lines. IV. Pressure Broadening of the Ammonia Inversion Spectrum", J. Chem. Phys., 50, No. 8, 3320 (1969).

18. J. Curtis, "Vibration-Rotation Bands of NH_3 in the region 670 cm^{-1}-1860 cm^{-1}", Ph.D. Dissertation, The Ohio State University, 1974.

19. F. Shimizu, "Stark Spectroscopy of PH_3 by 10 μm CO_2 and N_2O Lasers", J. Phys. Soc. Japan, 38, 293 (1975).

20. P. K. Yin and K. N. Rao, "ν_2 and ν_4 Fundamentals of Phosphine occurring at 8-12 μm", J. Mol. Spectrosc., 51, 199 (1974).

21. Y. Y. Kwan and E. A. Cohen, "Coriolis interaction Between ν_ℓ and $2\nu_n$ for Axially Symmetric Molecules of the Group C_3v, Application of Stark Effect of NH_3 in $v_4 = 1$ state," J. Molec. Specstrosc., 58, 54 (1975).

22. G. H. Herzberg, Infrared and Raman Spectra of Polyatomic Molecules, (Van Nostrand, New York, 1945) p. 425.

23. J. J. Tiee and C. Wittig, "CF_4 and NOCl Molecular Lasers Operating in the 16 μm Region" to be published.

3. PERSONNEL ASSOCIATED WITH GRANT AFOSR 76-2988

	Percent Time	
Paul D. Coleman, Professor EE Principle Investigator	5%	February 1, 1976- May 20, 1976
	30%	May 21, 1976- July 20, 1976
	5%	August 21, 1976- January 31, 1976
Edward J. Danielewicz Research Assistant	50%	February 1, 1976- May 20, 1976
	100%	May 21, 1976- August 20, 1976
William Lee Research Assistant	50%	May 21, 1976- July 20, 1976
	50%	August 21, 1976- January 31, 1977
Edward Malk Research Assistant	50%	February 1, 1976- July 20, 1976
	50%	August 21, 1976- January 31, 1977
Richard Ziolkowski Research Assistant	50%	February 21, 1976- July 20, 1976
Joseph Niesen Student Hourly	-	August 23, 1976- January 31, 1977
Donald S. Fulton Electronics Technician	20%	February 1, 1976- January 31, 1977
Jimmie H. Smith Secretary	20%	February 1, 1976- January 31, 1977

4. TECHNICAL ACTIVITIES

a) Attended and presented paper at the Integrated Optics Conference, Salt Lake City, Utah, January 12-14, 1976.

b) Visited Westinghouse Electric, Churchill, Pa., January 23, 1976.

c) Attended Conference on Lasers for Isotope Separation, Albuquerque, New Mexico, April 12-14, 1976.

d) Attended Workshop on Microfabrication Techniques, St. Louis, Missouri, May 2-3, 1976.

e) Attended Third Joint Strategic Science Meeting, San Diego, California, June 1-4, 1976.

f) Attended Device Research Conference, Salt Lake City, Utha, June 21-23, 1976.

g) Visited Honeywell Research Laboratories, Minneapolis, Minnesota, September 23, 1976.

h) Visited Harry Diamond Laboratories, Washington, D.C. December 15, 1976.

i) Attended and presented paper at the Second International Conference and Winter School on Submillimeter Waves and Their Applications, San Juan, Puerto Rico, December 6-10, 1976.

j) Chairman, IEEE Journal of Quantum Electronics Council.

k) Member of Industrial Affiliates Workshop Program Committee.

l) Treasurer, Device Research Conference, 1967 - present.

m) Member URSI, Commission I.

n) Review papers for APL, IEEE and JOA.

o) Review proposals for NSF and ARO.

p) Representative to Zenith, University of Illinois Industrial Affiliates Program.

5. LIST OF MANUSCRIPTS SUBMITTED TO A JOURNAL

a) "High-Power Vibration-rotation Emission from $^{14}NH_3$ Optically Pumped Off Resonance", with E. J. Danielewicz, E. G. Malk, Appl. Phys. Lett., 29, No. 9, 1 November 1976.

b) "Far Infrared Guided Wave Optics Experiments with Anisotropic Crystal Quartz Waveguides", with E. J. Danielewicz", submitted to the Journal of Quantum Electronics.

c) "Assignments of the High Power Optically Pumped CW Laser Lines of CH_3OH", with E. J. Danielewicz, submitted to the Journal of Quantum Electronics.

d) "Present and Future Problems in the Far IR", submitted to the Journal of the Optical Society.

6. LIST OF PAPERS PRESENTED AT MEETINGS

a) "Far Infrared Guided Wave Optics Experiments with Anisotropic Crystal Quartz Waveguides" Paper MC2, Topical Meeting on Integrated Optics, Salt Lake City, Utah, January 12-14, 1976.

b) "Assignments of the High Power Optically Pumped CW Laser Lines of CH_3OH, Presented at the Second International Conference and Winter School on Submillimeter Waves and Their Applications, San Juan, Puerto Rico, December 6-10, 1976.

c) "Present and Future Problems in the Far IR', presented at the Second International Conference and Winter School on Submillimeter Waves and Their Applications, San Juan, Puerto Rico, December 6-10, 1976.